Hover Dynamics and Flight Control of a UAM-Scale Quadcopter with Hybrid RPM and Collective Pitch Control

Ariel Walter*
Ph.D. Candidate

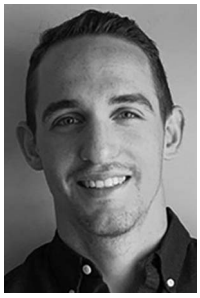

Michael McKay
Ph.D. Graduate

Robert Niemiec
Research Scientist

Farhan Gandhi
Redfern Professor, Director

Center for Mobility with Vertical Lift (MOVE), Rensselaer Polytechnic Institute, Troy, NY

Tom Berger
Flight Controls Group Lead
U.S. Army Combat Capabilities Development Command, Aviation & Missile Center, Moffett Field, CA

Hover analysis is performed on a 1200-lb gross weight UAM-scale quadcopter with both variable rotor speed and collective pitch control. With these redundant controls, the hover performance and flight dynamics are considered at three trim points, where power consumption can be increased to improve authority of the pitch inputs for changes in rotor thrust. An explicit model following control laws is optimized using CONDUIT® to meet ADS-33E-PRF handling qualities specifications, with design margin optimization on each axis. The responses of the linearized system are examined with either control type, and pitch control is shown to outperform RPM-control in heave, while the opposite is true for yaw. Trim in axial climb is simulated, where the collective pitch can be scheduled with the climb rate to maintain effective stall margin. Hybrid control mixing is implemented using a complementary filter, allowing the aircraft to use pitch control for short-term responses and RPM control for trim. The benefits of this hybrid control scheme are demonstrated through simulation of hot/high/heavy conditions, where trimming with RPM control allows the pitch actuators to maintain margin for maneuvers. It is concluded that hybrid control allows the aircraft to reap the benefits of pitch control for maneuverability while maintaining stall margin by using RPM control for trim.

Nomenclature

K	scaling factor
L	roll stability/control derivative
M	pitch stability/control derivative
N	yaw stability/control derivative
p	roll rate
q	pitch rate
r	yaw rate
T	time delay
T	rotor speed stability/control derivative
u, v, w	aircraft velocity (body frame)
U	control inputs
V	motor voltage
x, y, z	aircraft position (inertial frame)
X	dynamic states
X, Y, Z	velocity stability/control derivative
α	complementary filter cutoff frequency
α_{75}	angle of attack at 75% radius
δ	virtual acceleration input
ζ	damping ratio
θ	pitch attitude

*Corresponding author; email: waltea@rpi.edu.
Presented at VFS 78th Annual Forum, Fort Worth, TX, May 10–12, 2022.
Manuscript received October 2022; accepted March 2023

Θ	root pitch angle
τ	time constant
ϕ	roll attitude
ψ	heading
Ψ_k	rotor k azimuthal location
ω_N	natural frequency
Ω	rotor speed
ACAH	attitude command, attitude hold
DMO	design margin optimization
DRB	disturbance rejection bandwidth
DRP	disturbance refection peak
EMF	explicit model following
eVTOL	electric vertical takeoff and landing
ISA	International Standard Atmosphere
OLOP	open-loop-onset-point
RCDH	rate command, direction hold
RCHH	rate command, height hold
RMS	root mean square
RPM	rotations per minute
UAM	urban air mobility

Introduction

The development of Urban Air Mobility (UAM) programs has brought about a variety of technical challenges as novel electric vertical takeoff and landing (eVTOL) configurations and applications are being considered. One such challenge is ensuring satisfactory handling qualities. It has been previously shown that the fixed-pitch, variable rotations per minute (RPM) rotors traditionally used in small-scale vehicles are not as effective for control at larger scales, due to increased rotor inertia becoming a major factor influencing the aircraft dynamics and performance (Refs. 1–3). To maneuver such aircraft, the rotors must be accelerated quickly in order to produce the necessary changes in thrust, which results in spikes in motor current/torque as the system must overcome the rotor inertia. The effect of rotor inertia has been shown to increase with larger rotor sizes (Ref. 4), leading to relatively large, high-torque motors being required to meet handling qualities requirements (Ref. 1).

Rather than variable RPM, another option for control of multirotor aircraft is the use of variable collective feathering. Like the collective pitch input used on conventional rotorcraft, varying the root blade pitch allows changes in thrust without accelerating the rotors. In Ref. 2, Malpica and Withrow-Maser found that UAM-scale aircraft with collective pitch control were able to meet handling qualities requirements, but aircraft with rotor speed control could not due to assumed torque limitations. Niemiec et al. (Ref. 3) also considered both variable rotor speed and collective pitch control but found that both configurations were limited by the current required during yaw maneuvers, as these maneuvers rely directly on motor torque, which is proportional to current.

Theron et al. (Ref. 5) considered a hybrid control scheme with nonlinear dynamics inversion for a UAM-scale eVTOL. Utilizing a complementary filter for control mixing between variable RPM and variable pitch, the hybrid control scheme was not shown to provide any benefit over the collective pitch control alone. However, this study did not perform optimization of the control algorithm and only examined a subset of the standard handling qualities requirements defined in the ADS-33E-PRF (Ref. 6).

As shown by McKay et al. (Ref. 7), variable-RPM control can be more power efficient than variable-pitch control when considering changes in trim condition. The use of hybrid RPM and collective pitch control will allow the aircraft to utilize the faster pitch actuators for maneuvers and short-term responses while allowing the utilization of variable RPM for trim.

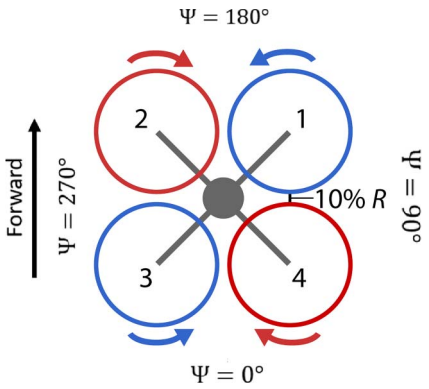

Fig. 1. Quadcopter configuration with rotor numbering.

Table 1. Aircraft parameters

Parameter	Value
Gross weight	1200 lb
Disk loading	6 psf
Rotor radius	4 ft
Rotor inertia	47 lb ft^2
Blade twist	−10.3°
Rotor solidity	0.09
Blade taper ratio	2.5

The goal of this study is to analyze the dynamics of a UAM-scale quadcopter with hybrid variable rotor speed and collective pitch control. The addition of feathering does not affect the ability of the motors to operate independently at different speeds, so each rotor's thrust can be regulated in two ways. With this redundancy in control, several trim points can be considered, and the resulting changes in linear dynamics analyzed. Then, optimized explicit-model-following (EMF) controllers can be designed using CONDUIT® to meet standard ADS-33E-PRF (Ref. 6) handling qualities specifications. Aircraft performance can then be compared with either variable-RPM control, variable-pitch control, or a combination of both utilizing a complementary filter for control mixing.

Modeling and Analysis Tools

Platform

A hybrid variable-RPM and variable-pitch control scheme are applied to a quadcopter with a gross weight of 1200 lb, similar to the aircraft in Ref. 1. Each rotor is directly driven by an electric motor with actuation of the root pitch of the blades. The aircraft is flown in a cross-configuration and has 10% rotor radius tip clearance with rotor numbering as shown in Fig. 1. Other basic aircraft parameters are listed in Table 1, along with rotor geometry. The airfoil sections are NACA4412 at the root of the blade and Clark Y at the tip, with a linear interpolation between (as in Ref. 7). Rotor inertia is determined based on a curve fit to existing rotor data described in Ref. 1.

Simulation models

Aircraft dynamics are modeled using the Rensselaer Multicopter Analysis Code (Ref. 8), which calculates the forces and moments on the quadcopter using blade element theory coupled with a 3 × 4 Peter–He finite state dynamic wake model (Ref. 9). The linearized dynamic states include the 12 rigid-body states (position, attitude, linear velocity,

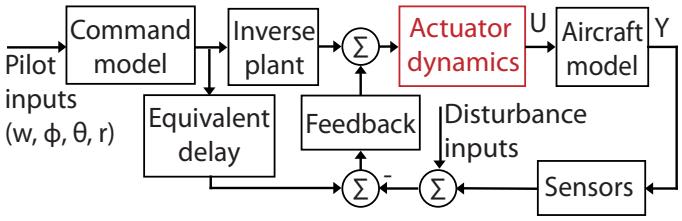

Fig. 2. EMF control architecture.

and angular rate), 10 inflow states per rotor (40 total), and the four rotor speeds for a total of 56 states. Since the inflow states are generally very high frequency (Ref. 10), these states can be assumed to settle instantaneously and reduced out of the linear model via static condensation, yielding a reduced-order model with states listed in Eq. (1). Each rotor has two inputs: a voltage signal to the motor and a root pitch angle, for a total of eight inputs to the aircraft (Eq. (2)).

$$\mathrm{X} = [x \;\; y \;\; z \;\; \phi \;\; \theta \;\; \psi \;\; u \;\; v \;\; w \;\; p \;\; q \;\; r \;\; \Omega_1 \;\; \Omega_2 \;\; \Omega_3 \;\; \Omega_4]^T \tag{1}$$

$$\mathrm{U} = [V_1 \;\; V_2 \;\; V_3 \;\; V_4 \;\; \Theta_1 \;\; \Theta_2 \;\; \Theta_3 \;\; \Theta_4]^T \tag{2}$$

Control mixing is defined using a multirotor coordinate transform (Eq. (3); Ref. 11), where Ψ_k represents the azimuthal location of rotor hub k (Fig. 1, Eq. (4)). This transform is applied to the voltage inputs in Eq. (3), where V_0 represents mean voltage, used to control the heave axis. V_{1s}/V_{1c} represent lateral/longitudinal variation in voltage input and thus control roll/pitch. Finally, V_d alternates sign with the rotor rotational direction, producing a yaw moment on the aircraft. The same transform is used for the pitch inputs, defining Θ_0, Θ_{1c}, Θ_{1s}, and Θ_d. Using the multirotor coordinate transform decouples the dynamics of the quadcopter, resulting in two inputs (voltage and root pitch) that affect each of the four aircraft axes.

$$\begin{bmatrix} V_1 \\ V_2 \\ V_3 \\ V_4 \end{bmatrix} = \begin{bmatrix} 1 & \sin(\Psi_1) & \cos(\Psi_1) & 1 \\ 1 & \sin(\Psi_2) & \cos(\Psi_2) & -1 \\ 1 & \sin(\Psi_3) & \cos(\Psi_3) & 1 \\ 1 & \sin(\Psi_4) & \cos(\Psi_4) & -1 \end{bmatrix} \begin{bmatrix} V_0 \\ V_{1s} \\ V_{1c} \\ V_d \end{bmatrix} \tag{3}$$

$$\Psi_k = (90k + 45)^\circ \quad \text{for} \quad k = 1, 2, 3, 4 \tag{4}$$

Controller architecture

Like the inner loop in Ref. 1, a rate-command-height-hold/attitude-command-attitude-hold/rate-command-direction-hold (RCHH/ACAH/RCDH) EMF control architecture is implemented to stabilize and control the aircraft in hover (Fig. 2).

Pilot heave rate, roll/pitch attitude, and yaw rate inputs are passed through a command filter (first order for heave and yaw, second order for roll and pitch). The feedforward path consists of an inverse of an approximated aircraft dynamics model, while the feedback path includes an equivalent delay that accounts for the effects of the actuator and sensor dynamics (excluded from the approximated model inverse). A sensor delay is included on the output signals from the simulation model (as in Ref. 12), and proportional–integral–derivative (PID) feedback control is implemented to stabilize the vehicle, mitigate errors, and reject disturbances.

The sum of the feedforward and feedback paths is designed as a virtual acceleration command δ for each axis, rather than specifically a rotor speed or blade pitch input:

$$\delta = [\delta_0 \;\; \delta_{1s} \;\; \delta_{1c} \;\; \delta_d].^T \tag{5}$$

This allows each aircraft axis to be treated as a single-input-single-output (SISO) system despite having two control inputs (motor voltage and root pitch in multirotor coordinates). Control mixing for the hybrid control system takes this input acceleration command for each axis and outputs both the motor voltages (RPM control) and blade pitches (pitch control) to give input U (Eq. (2)) to the simulation model.

The hybrid control mixer is illustrated by the block diagram in Fig. 3. The acceleration command δ for each multirotor input is split into two paths: one corresponding to the rotor speed control path and the other corresponding to the blade pitch control path. Appropriate scaling is applied to input δ based on the bare-airframe dynamics (explained in the next section) and then passed through a complementary filter.

The complementary filter separates the signal into high- and low-frequency content, taking the form

$$\text{High pass} = \frac{s}{s+\alpha}, \quad \text{Low pass} = \frac{\alpha}{s+\alpha}. \tag{6}$$

For each rotor, the blade pitch actuator receives the high-frequency (maneuver) content, while the low-frequency (trim) content is allocated to the motor speed controller. This will essentially allow the aircraft to use changes in blade pitch for short-term responses, such as the acceleration at the beginning of a maneuver, while the rotor speed is used for longer responses, such as changes in trim condition.

The complementary filter cutoff frequency α dictates the frequency at which the transition from RPM control to pitch control occurs, illustrated in Fig. 4. For frequencies less than α, the low-pass path has higher gain, while for frequencies greater than α, the high-pass path has higher gain. For frequencies further than a decade from α, the frequency content is effectively routed entirely to either the low- or high-pass path. When summed together, the low- and high-pass filters result in 0 dB (unity) gain and 0° phase lag for all frequencies. Lower values of α will route relatively more content to the high-pass (pitch-control) path, allowing the rotor speed to change more slowly.

Figure 5 demonstrates how the rotor speed and blade pitch inputs are affected by the complementary filter cutoff frequency of the hybrid controller when commanding an increase in rotor thrust. First considering pure pitch control ($\alpha = 0$, blue in Fig. 5), only changes in blade pitch are used to produce the change in thrust, while the rotor speed is held at the nominal value. With low complementary filter cutoff frequency ($\alpha = 0.1$, red Fig. 5), the pitch actuator is used for the initial response, but in the long-term responses, the rotor speed slowly increases while

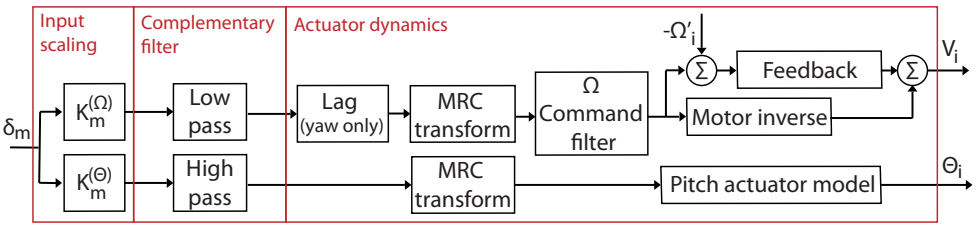

Fig. 3. Hybrid control mixing and actuator dynamics.

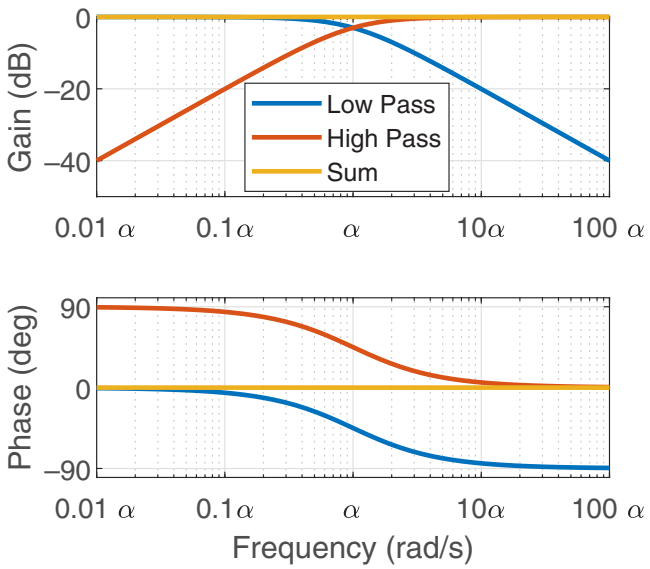

Fig. 4. Complementary filter frequency response.

the blade pitch decreases to maintain the desired thrust until the blade pitch has been reduced to its nominal value. This transition happens more rapidly as α increases. As α approaches infinity, the pitch actuator remains unperturbed and the change in thrust is produced purely with changes in rotor speed. The same net thrust is produced throughout the simulation independent of the value of α, which only influences how the change in thrust is distributed between the rotor speed and blade pitch actuators as time progresses.

After passing through the complementary filter, both paths are transformed into individual rotor coordinates before going to the actuator dynamics. Another EMF control loop is implemented on the rotor speed. Though the motor dynamics model can be perfectly inverted (Ref. 4), feedback control on the rotor speed is included in order to account for the effects of changing blade pitch, similar to an engine governor or electronic speed controller. This drives any changes in rotor speed to zero when pure collective pitch control is being considered. Pitch actuator dynamics are included in the blade pitch control path. The pitch actuators are assumed to be second order with an assumed damping ratio of $\zeta = \sqrt{2}/2$ and natural frequency of $\omega_N = 82$ rad/s:

$$G_\Theta = \frac{\Theta}{\Theta_{cmd}} = \frac{\omega_N^2}{s^2 + 2\zeta\omega_N s + \omega_N^2} \tag{7}$$

This model is based on a Froude scaling of the UH-60A tail rotor actuator model presented in Ref. 13. The pitch actuator also includes a rate limit of 20 deg/s and maximum root pitch of 24° to avoid stall.

Hover dynamics and input scaling

Scaling of the acceleration inputs ($K^{(\Omega)}$ and $K^{(\Theta)}$ in Fig. 3) for each axis is determined based on analysis of the bare-airframe dynamics, assuming the rotor speed control loop is closed. With the use of multirotor coordinates, the linearized hover model can be split into independent models for each axis. The dynamics of each axis are broken down to examine the sensitivity to changes in rotor speed or blade pitch and determine the appropriate input scaling. Scaling by the inverse of the individual control derivatives eliminates them entirely from the vehicle dynamics. Though this method is similar to using a pseudoinverse of the hybrid control dynamics, it differs due to the complementary filter.

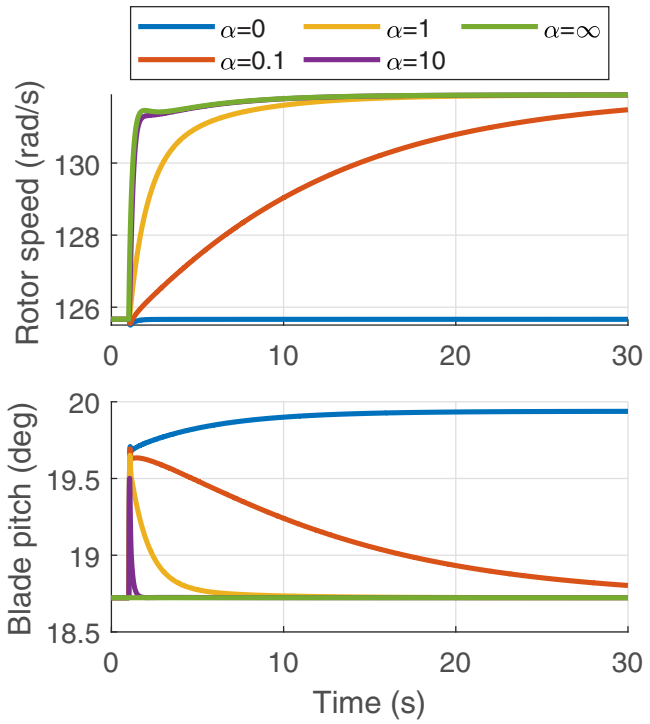

Fig. 5. Rotor speed and pitch inputs with complementary filter.

Absent the complementary filter, the pseudoinverse would eliminate the control derivatives, but since the complementary filter splits the input up based on frequency, the pseudoinverse is not appropriate.

The heave dynamics can be represented by

$$\begin{bmatrix} \dot{w} \\ \dot{\Omega}_0 \end{bmatrix} = \begin{bmatrix} Z_w & Z_\Omega \\ T_w & T_\Omega \end{bmatrix} \begin{bmatrix} w \\ \Omega_0 \end{bmatrix} + \begin{bmatrix} 0 & Z_\Theta \\ T_V & T_\Theta \end{bmatrix} \begin{bmatrix} V_0 \\ \Theta_0 \end{bmatrix} \tag{8}$$

with the heave rate and collective rotor speed as states and the collective voltage and collective blade pitch as inputs. The rotor torque produced from changes in heave rate (T_w) and collective blade pitch (T_θ) is negligible. Thus, the heave model can be simplified to get

$$\dot{w} = Z_w w + Z_\Omega \Omega_0 + Z_\theta \Theta_0 \tag{9}$$

From these simplified dynamics (without actuator dynamics), the main difference in heave response from changes in rotor speed versus changes in blade pitch is a difference in gain (Z_Ω vs. Z_Θ). Thus, the inverse of these values is used to scale the heave acceleration input for the corresponding control path.

Since the roll and pitch dynamics of the vehicle are nearly identical (the only difference being a difference in fuselage inertia), only the pitch model is presented. The linearized pitch dynamics model is

$$\begin{bmatrix} \dot{\theta} \\ \dot{u} \\ \dot{q} \\ \dot{\Omega}_{1c} \end{bmatrix} = \begin{bmatrix} 0 & 0 & 1 & 0 \\ -g & X_u & X_q & 0 \\ 0 & M_u & M_q & M_\Omega \\ 0 & 0 & T_q & T_\Omega \end{bmatrix} \begin{bmatrix} \theta \\ u \\ q \\ \Omega_{1c} \end{bmatrix} + \begin{bmatrix} 0 & 0 \\ 0 & 0 \\ 0 & M_\Theta \\ T_V & T_\Theta \end{bmatrix} \begin{bmatrix} V_{1c} \\ \Theta_{1c} \end{bmatrix} \tag{10}$$

Several effects within this model are negligible, and the pitch dynamics can be simplified with the assumption that $X_q = T_q = T_\Theta = 0$. Rewriting the third row of Eq. (10) gives

$$\dot{q} = M_u u + M_q q + M_\Omega \Omega_{1c} + M_\theta \Theta_{1c} \tag{11}$$

Table 2. Input scaling

	Heave	Roll	Pitch	Yaw
$K^{(\Omega)}$	$1/Z_\Omega$	$1/L_\Omega$	$1/M_\Omega$	T_V/N_V
$K^{(\Theta)}$	$1/Z_\Theta$	$1/L_\Theta$	$1/M_\Theta$	$-T_V/(N_V T_\Theta)$

From this, the difference in gain between pitch response from changes in rotor speed versus changes in blade pitch (M_Ω vs. M_Θ) is identified, with the inverse of these values used to scale the pitch acceleration input.

The linearized yaw dynamics include the yaw rate and differential rotor speed as states and the differential motor voltage and differential blade pitch as inputs:

$$\begin{bmatrix} \dot{r} \\ \dot{\Omega}_d \end{bmatrix} = \begin{bmatrix} N_r & N_\Omega \\ T_r & T_\Omega \end{bmatrix} \begin{bmatrix} r \\ \Omega_d \end{bmatrix} + \begin{bmatrix} N_V & 0 \\ T_V & T_\Theta \end{bmatrix} \begin{bmatrix} V_d \\ \Theta_d \end{bmatrix} \tag{12}$$

The input scaling for the yaw axis must be handled differently than the thrust-dominated axes, as yaw differs notably from heave and roll/pitch in two ways:

1) Pitch inputs do *not* have any direct impact on the yaw acceleration of the vehicle. Instead, pitch inputs produce a yaw moment indirectly through the motor dynamics. Thus, the effect of rotor pitch on the rotor speed cannot be ignored.

2) The motor voltage has a direct effect on the yaw rate. When a change in Ω_d is commanded, V_d changes to meet that command, and the vehicle will yaw immediately (leading the motor response).

Of all of the derivatives in Eq. (12), only the effect of the yaw rate on rotor acceleration (T_r) can be neglected. Input scaling parameters can be obtained by assuming perfect tracking of Ω_d ($\Omega_d = \Omega_{d,cmd}$). The second row of Eq. (12) becomes

$$\dot{\Omega}_d = T_\Omega \Omega_d + T_\Theta \Theta_d + T_V V_d, \quad V_d = \frac{(s - T_\Omega)\Omega_d}{T_V} - \frac{T_\Theta \Theta_d}{T_V} \tag{13}$$

Substitution into the first row of Eq. (12) yields

$$(s - N_r)r = \frac{N_v}{T_V}\left(s - T_\Omega + \frac{N_\Omega T_V}{N_V}\right)\Omega_d - \frac{N_V T_\Theta}{T_V}\Theta_d \tag{14}$$

To account for the direct effect of voltage on yaw rate, consider the transfer function from commanded differential rotor speed ($\Omega_{d,cmd}$) to yaw rate (r), which takes the form

$$\frac{r}{\Omega_{d,cmd}} = \frac{N_V}{T_V}\left(s - T_\Omega + \frac{N_\Omega T_V}{N_V}\right) C_\Omega \frac{1}{s - N_r} \tag{15}$$

where the zero represents the lead introduced by the voltage's immediate effect on the motor reaction torque and C_Ω represents the motor speed command filter in Fig. 3. By adding a lag filter to cancel out the zero, the yaw response becomes a simple first-order transfer function, multiplied by the rotor speed command model. A summary of the input scaling is presented in Table 2.

Hybrid control mixing

A key component of the EMF control architecture (Fig. 2) is an invertible model approximation. This approximation is relatively straightforward when considering pure RPM or pitch control. For example, considering the heave axis with RPM control, the model inverse uses the heave damping (Z_w), a gain (Z_Ω), and an equivalent delay to approximate the effects of the actuator dynamics (Ω/V).

When considering hybrid control mixing, the inverse model must approximate the acceleration command (δ) needed to produce the desired vehicle response. Both the RPM- and pitch-control paths contribute to this. Again using the heave axis as an example, the block diagram shown in Fig. 3 combined with the aircraft model (Eq. (9)) can be represented as a transfer function:

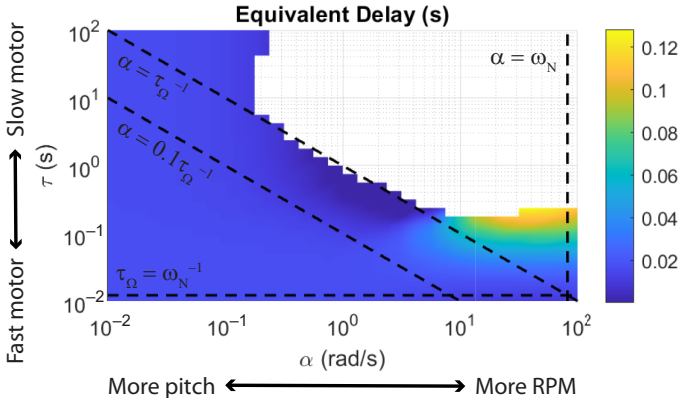

Fig. 6. Optimal equivalent delay.

$$G_0 = \frac{w}{\delta_0} = \frac{1}{(s - Z_w)(s + \alpha)}\left(\underbrace{\frac{\alpha}{\tau_\Omega s + 1}}_{\text{RPM path}} + \underbrace{\frac{\omega_N^2 s}{s^2 + \zeta\omega_N s + \omega_N^2}}_{\text{Pitch path}}\right)$$

$$= \frac{1}{(s - Z_w)} \frac{\alpha\tau_\Omega^{-1}\left(s^2 + 2\zeta\omega_N s + \omega_N^2\right) + \omega_N^2 s\left(s + \tau_\Omega^{-1}\right)}{(s + \alpha)\left(s + \tau_\Omega^{-1}\right)\left(s^2 + 2\zeta\omega_N s + \omega_N^2\right)} \tag{16}$$

With the complementary filter, the hybrid control heave dynamics become a two-zero, four-pole system with a pole at the cutoff frequency. As α approaches zero, the motor pole (τ_Ω^{-1}) will reduce out and only the pitch actuator will be used, while as α approaches infinity the pitch actuator dynamics will cancel out and only the rotor speed will be used for control.

With the input scaling from Table 2, the effective gain from the plant is 1 and the hybrid control model is approximated by

$$\tilde{G}_0 = \frac{1}{(s - Z_w)} e^{-s\mathrm{T}(\alpha, \tau_\Omega)} \tag{17}$$

A delay $\mathrm{T}(\alpha, \tau_\Omega)$ is included in order to approximate the effects of the mixed motor and pitch actuator dynamics. Since the pitch actuator model is fixed (Eq. (7)), the delay is considered a function of the complementary filter cutoff frequency α and motor speed time constant τ_Ω.

With different values of α and τ_Ω, the equivalent delay (T) is identified to minimize the difference in frequency response between the hybrid control plant (Eq. (16)) and approximation (Eq. (17)) for a frequency range of 0.1 to 10 rad/s. The delay is plotted in Fig. 6, where the values are cut off when the model following cost between the plant and approximation exceeds 50 (according to guidelines in Ref. 14).

Several key locations are indicated in Fig. 6 by dashed lines, the significance of which is summarized:

1) $\alpha > \omega_N$: Input to the pitch control path is faster than the pitch actuator can adequately follow, effectively reducing the system to only RPM control.

2) $\alpha > 0.1\tau_\Omega^{-1}$: Input to the RPM path begins to include content faster than the motor can adequately follow. As α approaches τ_Ω^{-1}, more content is routed to the motors that is higher frequency than they havethe bandwidth to adequately follow.

3) $\tau_\Omega < \omega_N^{-1}$: Motor is required to respond faster than the pitch actuator, which is unlikely in practice and will not be considered in this study.

Despite improving motor response times, smaller values of τ_Ω generally lead to higher required motor current as a result of the higher required

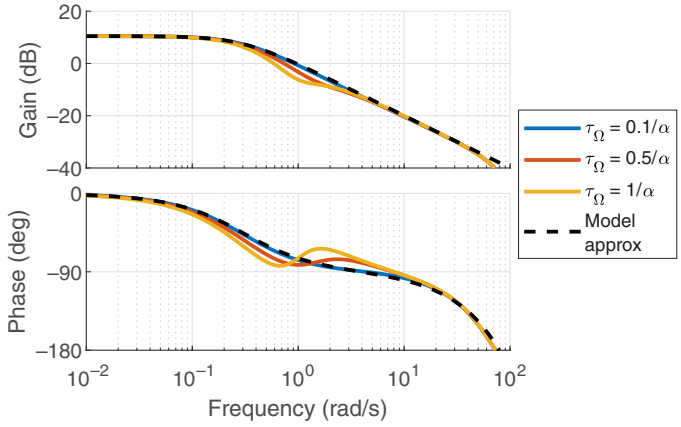

Fig. 7. Plant approximation for $\alpha = 1$.

acceleration. However, values of τ_Ω above $0.1/\alpha$ can cause the zero in Eq. (16) to have a noticeable effect on the frequency response, reducing the accuracy of the model approximation. This behavior is illustrated in Fig. 7 for a cutoff frequency of 1 rad/s and becomes less pronounced at smaller and larger values of α as the system moves more toward pure RPM or pitch control. As α increases past 10 or decreases past 0.1, the zero behavior is pushed out of the frequency range of interest for the model following, so $\tau_\Omega > 0.1\alpha$ can be considered. The model following with $\tau_\Omega > 0.1\alpha$ could be improved by considering a higher order inverse approximation.

When using primarily pitch control for maneuvers ($\alpha \leq 1$), the value of the motor time constant can be fixed to $0.1/\alpha$. This value will give the motor adequate authority to follow commands from the low-pass filter. Further reducing the value of τ_Ω will have no effect on the system, since the motor response will be dominated by the low-pass filter. From Fig. 6, the value of the delay for the model approximation is fixed at T = 20 ms, as this should provide an adequate model following at high frequency, as long as $\alpha \leq \tau_\Omega^{-1}$. This value is driven by the delay from the pitch actuator, which is used for the high-frequency response.

Control optimization

As recommended in Ref. 12, the remaining control system parameters (feedback gains) are optimized in CONDUIT® to meet a comprehensive set of stability, handling qualities, and performance requirements (Table 3). The optimization routine seeks to minimize the actuator effort (defined by the summed objectives), without violating any hard (stability) or soft (performance) constraints that are designed to ensure satisfactory handling qualities.

In addition to several ADS-33E-PRF hover and low-speed requirements (Ref. 6) such as piloted bandwidth and minimum damping ratios, disturbance rejection requirements (Ref. 15), and open-loop onset point (OLOP; Ref. 16) actuator rate limiting specifications are also included. In addition to typical actuator root mean square (RMS) objective functions, additional objective functions associated with the motor current during heave, pitch, and yaw step responses are included. These are included with the aim of minimizing the peak current during maneuvers as well as to impose a limit on the maximum current allowed to the motors (constrained to be less than twice the hover current). To evaluate whether current limits are violated, "maximum" inputs for each axis are defined: a step with a magnitude of $w = -3.8$ m/s for heave, $\phi/\theta = 20^\circ$ for roll/pitch, and $r = 20$ deg/s for yaw.

After meeting standard handling qualities metrics, design margin optimization (DMO) is performed by incrementally increasing the requirements in order to produce a family of Pareto-optimal controllers that provide improved maneuverability with minimal increase in actuator activity. This is done by moving the effective Level 1/2 boundary into the Level 1 region by a percentage of the width of the Level 2 region. For each axis, the design margin is applied to the bandwidth, crossover frequency, and disturbance rejection bandwidth. The design margin is increased until actuator rate (OLOP or maximum current) or position (maximum blade pitch) limits are reached. The margin is then reduced to 70% of the maximum value, as recommended by Ref. 12.

Table 3. CONDUIT® constraints

Specification	Type	Axes
Eigenvalues	Hard	All
Stability margins	Hard	All
Nichols margin	Hard	All
Bandwidth and phase delay	Soft	Roll, pitch, yaw
Crossover frequency	Soft	All
Disturbance rejection bandwidth	Soft	All
Disturbance rejection peak	Soft	All
Damping	Soft	All
Heave mode and delay	Soft	Heave
Model following cost	Soft	All
OLOP (pilot input and disturbance)	Soft	All
Actuator RMS (pilot input and disturbance)	Objective	All
Crossover frequency	Objective	All
Motor current minimization	Objective	All

An example of the trade-offs associated with DMO is demonstrated in Fig. 8 for the heave axis. Several handling qualities metrics are plotted with example values of design margin for the quadcopter operating with pitch control from the standard trim point. Black lines denote the nominal Level 1/2 and 2/3 boundaries for each specification. The Level 1/2 boundary for the heave crossover frequency, disturbance rejection bandwidth, and heave mode requirements are increased further into the Level 1 region as the design margin increases. This increase in design margin is associated with increased agility and controllability but also results in increased values of the OLOP specifications and maximum blade pitch during a heave maneuver towards the Level 2 boundary. For this case, the OLOP specification associated with disturbance inputs reaches the Level 1/2 boundary at a design margin of around 1.5 (150%). This is considered the limit of the DMO, as a further increase in the design margin is not possible without violating the OLOP specification. The final optimized heave controller for this case is chosen at 70% of the maximum, indicated by the star in Fig. 8 with a heave design margin of 1.1 (110%).

Results

Hover trim analysis

In hover, collective inputs are used to trim the aircraft, and with two inputs governing the heave axis, infinite trim solutions exist. The choice of hover trim point affects the dynamics, control authority, and power consumption of the aircraft.

The hover trim space is explored by sweeping through prescribed rotor speeds and solving for the required collective motor voltages and blade pitches. Starting at a tip speed of Mach 0.6 (1620 RPM), the rotor speed is decreased until the required blade pitch becomes high enough to stall. The resulting power and corresponding root pitch settings are plotted in Fig. 9. Stall becomes an issue around 24° root pitch (indicated by a dashed line) and is chosen as the upper limit of the blade pitch.

Some margin needs to be included in hover to avoid stall during maneuvers. An appropriate margin can be estimated from heave bandwidth

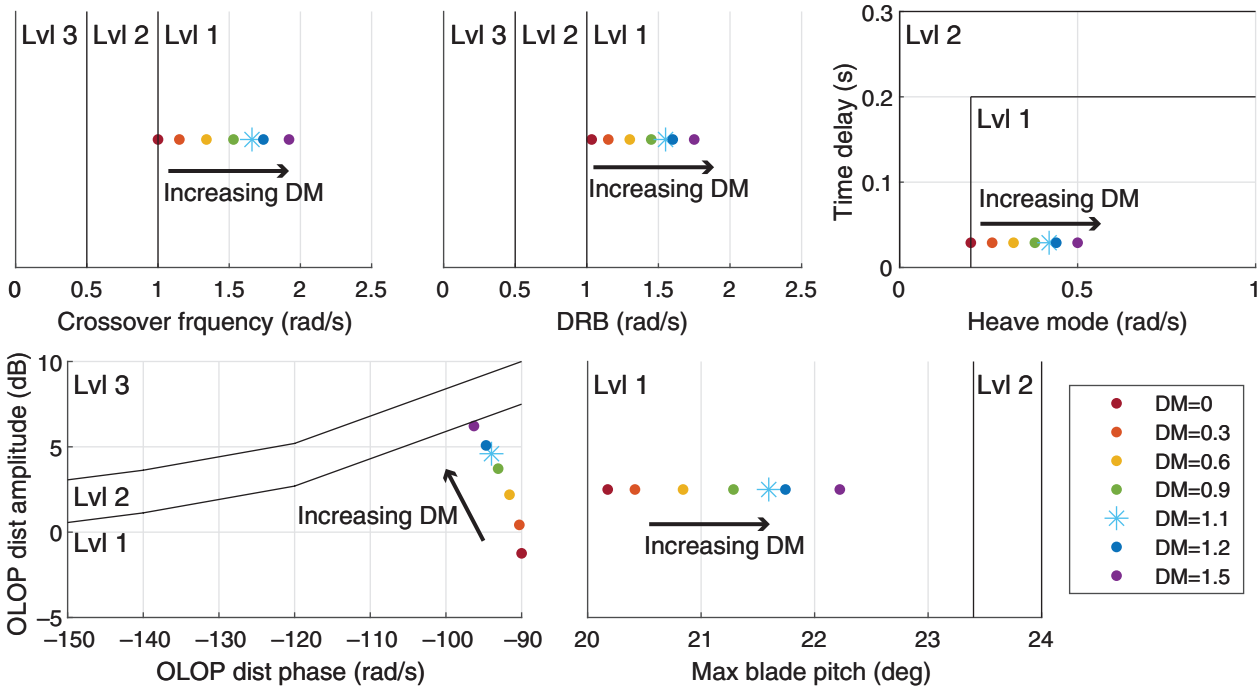

Fig. 8. Design margin trade-offs for heave axis.

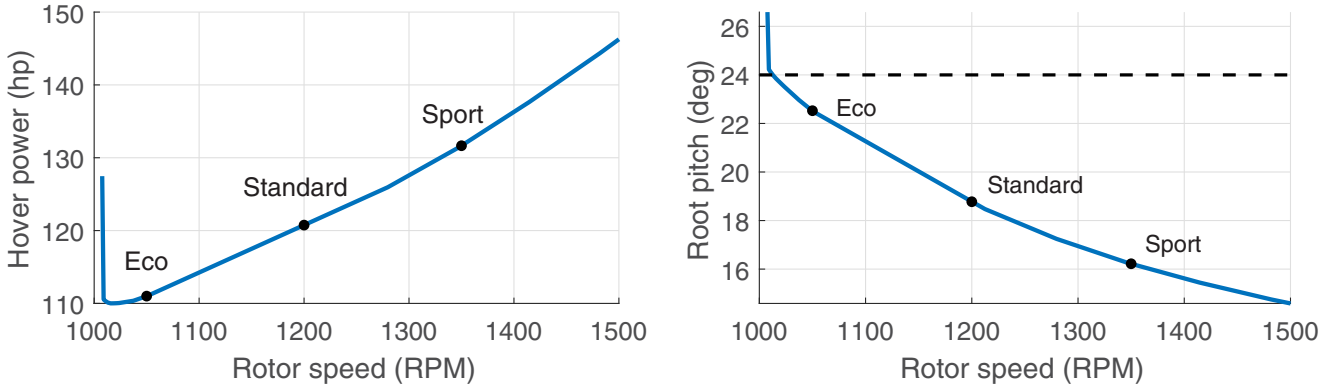

Fig. 9. Hover trim power and blade pitch input.

requirements and an assumed maximum climb rate. Assuming a first-order response type as prescribed by ADS-33E-PRF (Ref. 6), the heave response is represented as

$$w(t) = w_\infty(1 - e^{-t/\tau}) \tag{18}$$

for commanded heave rate w_∞ and time constant τ. From the derivative of heave rate,

$$\dot{w}(t) = w_\infty(e^{-t/\tau})/\tau \implies \dot{w}_{\max} = w_\infty/\tau \tag{19}$$

the maximum heave acceleration is w_∞/τ at $t = 0$. Based on the hover and low-speed requirements in ADS-33E-PRF, the maximum allowable heave time constant is $\tau = 5$ s. Thus, maximum heave acceleration (assuming unlimited power) can be determined by dividing the desired maximum heave rate by τ.

With variable-pitch control during a heave maneuver, the rotors will increase root pitch in order to quickly create the additional thrust to accelerate the aircraft upward. In order to find the maximum heave rate, the root pitch is assumed to increase to the maximum of 24° during the initial acceleration. Based on the additional force produced, the maximum heave acceleration and corresponding maximum heave rate are calculated from an assumed hover trim point.

Table 4. Hover trim points

	Eco	Standard	Sport
Rotor speed (RPM)	1050	1200	1350
Collective blade pitch (deg)	22.5	18.7	16.2
Total hover power (hp)	111	121	132
Maximum heave rate (ft/min)	760	4080	7940

Three hover trim points are chosen in order to analyze the differences in heave dynamics (black dots in Fig. 9). Hover trim rotor speeds of 1050 RPM (Eco), 1200 RPM (Standard), and 1350 RPM (Sport) are chosen, and corresponding blade pitch, hover power, and maximum heave rate (based on maximum achievable acceleration) are given in Table 4. The trim point with the least stall margin corresponds to a maximum heave rate of 3.8 m/s (760 ft/min), which far exceeds the ADS-33E-PRF requirement of 160 ft/min.

These trim points are labeled “Eco”, “Standard.” and “Sport” based on their trim power consumption. The increase in trim power at higher

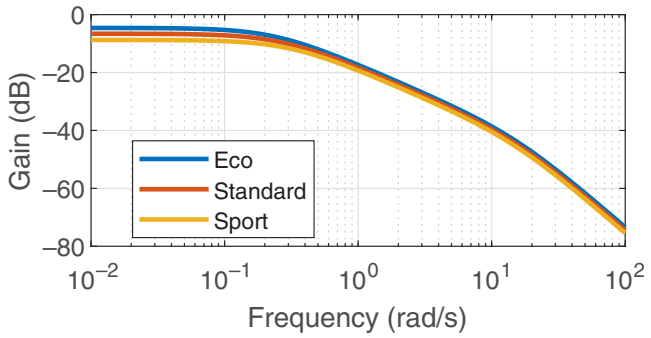

Fig. 10. Magnitude frequency response of motor voltage input to heave rate ($|w/V_0|$).

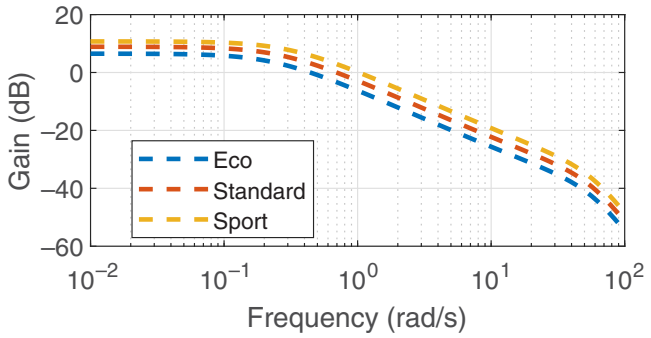

Fig. 11. Magnitude frequency response of blade pitch input to heave rate ($|w/\Theta_{0,cmd}|$).

Table 5. Heave stability and control derivatives

Trim Point	Z_w	Z_Ω	Z_Θ	T_Ω	T_V
Eco	−0.228	−0.184	−0.573	−15.5	11.7
Standard	−0.267	−0.163	−0.834	−15.2	11.7
Sport	−0.312	−0.146	−1.163	−15.1	11.7

trim rotor speed comes with an increase in stall margin, and therefore an improvement in expected agility and maneuverability when using pitch control for maneuvers.

Bare-airframe dynamics

To quantify the changes in agility, the bare air-frame dynamics are analyzed about the three different trim points with either RPM- or pitch-control inputs.

Linearized heave dynamics. First, considering the heave dynamics from Eq. (9), the two-state, two-input heave model can be represented by two SISO transfer functions when considering pure rotor speed or pure collective pitch control. These transfer functions can be further broken down into rigid body dynamics (w/Ω_0 or w/Θ_0) and actuator dynamics (Ω_0/V_0 or $\Theta_0/\Theta_{0,cmd}$):

$$\frac{w}{V_0} \approx \underbrace{\frac{Z_\Omega}{(s+Z_w)}}_{w/\Omega_0} \underbrace{\frac{T_V}{(s+T_\Omega)}}_{\Omega_0/V_0}, \quad \frac{w}{\Theta_{0,cmd}} \approx \underbrace{\frac{Z_\Theta}{(s+Z_w)}}_{w/\Theta_0} \underbrace{G_\Theta}_{\Theta_0/\Theta_{0,cmd}}. \tag{20}$$

The values of the heave stability and control derivatives for each of the hover trim points are given in Table 5. With increasing trim rotor speed, the heave subsidence mode (Z_w) increases in frequency. This is a result of the increased sensitivity of thrust to changes in heave rate at higher rotor speeds.

At higher trim rotor speed, heave acceleration (thrust) becomes less sensitive to changes in rotor speed (shown by a reduction in the magnitude of Z_Ω) but more sensitive to changes in collective blade pitch (shown by an increase in a magnitude of Z_Θ). Though the effect is small, this can be seen in the changes in low-frequency gain that occurs with different trim points (Figs. 10 and 11). With RPM control (Fig. 10), at higher frequency the difference between the trim points decreases, due to Z_w scaling similarly to $1/Z_\Omega$. For pitch control (Fig. 11), the difference in gain is consistent across the frequency range.

As shown in Fig. 12, the choice of trim point has very little effect on the phase response, with notable differences resulting from the relative lag between the motor pole and pitch actuator bandwidth. With motor voltage input (rotor speed control), the phase rolls off by 90° due to the motor pole, while with blade pitch control the phase rolls off by 180° (due to the second-order pitch actuator) at the higher frequency of the pitch actuator dynamics. Though the stability derivatives change with trim point, it is not enough to have a significant effect on the phase response.

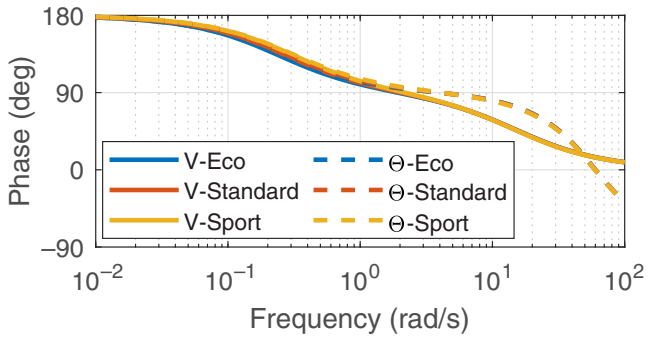

Fig. 12. Phase frequency response of collective input to heave rate ($\angle w/V_0$ and $\angle w/\Theta_{0,cmd}$).

Linearized roll/pitch dynamics. Due to the symmetry of the quadcopter platform, the roll and pitch dynamics are characteristically similar, so only the pitch dynamics are discussed in detail. Like heave, the roll/pitch dynamics of the aircraft (Eq. (11)) can be represented by two SISO transfer functions when considering pure RPM or pitch control. The transfer functions for both control types share a pole (p_1), zero (z_1), and unstable phugoid mode ($s^2 - 2\zeta_{ph}\omega_{ph}s + \omega_{ph}^2$). These transfer functions can be broken down into rigid body (θ/Ω_{1c} or θ/Θ_{1c}) and actuator dynamics (Ω_{1c}/V_{1c} or $\Theta_{1c}/\Theta_{1c,cmd}$):

$$\begin{aligned} \frac{\theta}{V_{1c}} &\approx \underbrace{\frac{M_\Omega(s+z_1)}{(s+p_1)\left(s^2-2\zeta_{ph}\omega_{ph}s+\omega_{ph}^2\right)}}_{\theta/\Omega_{1c}} \underbrace{\frac{T_V}{(s-T_\Omega)}}_{\Omega_{1c}/V_{1c}}, \\ \frac{\theta}{\Theta_{1c,cmd}} &\approx \underbrace{\frac{M_\Theta(s+z_1)}{(s+p_1)\left(s^2-2\zeta_{ph}\omega_{ph}s+\omega_{ph}^2\right)}}_{\theta/\Theta_{1c}} \underbrace{G_\Theta}_{\Theta_{1c}/\Theta_{1c,cmd}} \end{aligned} \tag{21}$$

The stability and control derivatives for the pitch axis are listed in Table 6. The values of T_Ω and T_V are not listed because they are the same as the values in Table 5. As shown in Fig. 13, the pole locations vary with the trim point. The choice of trim point has little effect on the phugoid mode but does affect the location of the subsidence mode.

The trim point also affects the low-frequency gain. Similar to the trends seen for the heave axis, at higher rotor speed the pitch rate becomes

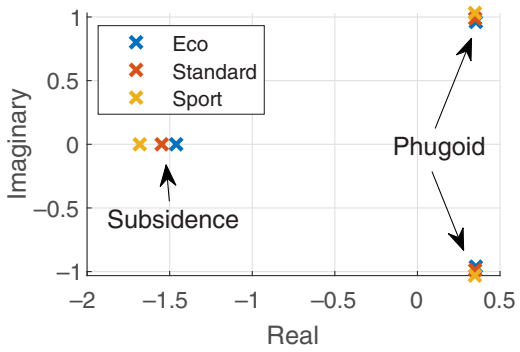

Fig. 13. Poles of bare-airframe pitch dynamics.

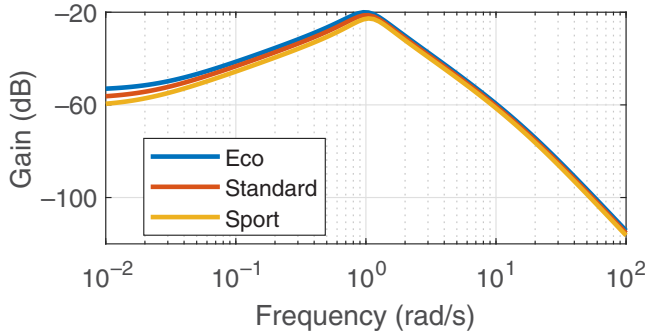

Fig. 14. Magnitude frequency response of motor voltage input to pitch attitude ($|\theta/V_{1c}|$).

Table 6. Pitch stability and control derivatives

Trim Point	X_u	M_u	M_q	M_Ω	M_Θ
Eco	−0.025	0.16	−0.71	−0.17	−0.52
Standard	−0.021	0.17	−0.83	−0.15	−0.75
Sport	−0.018	0.20	−0.97	−0.13	−1.05

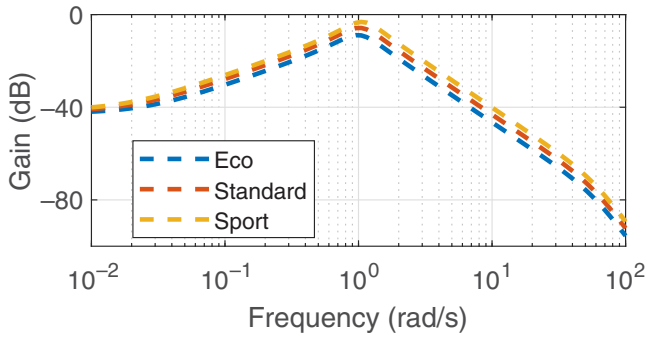

Fig. 15. Magnitude frequency response of blade pitch to pitch attitude ($|\theta/\Theta_{1c,cmd}|$).

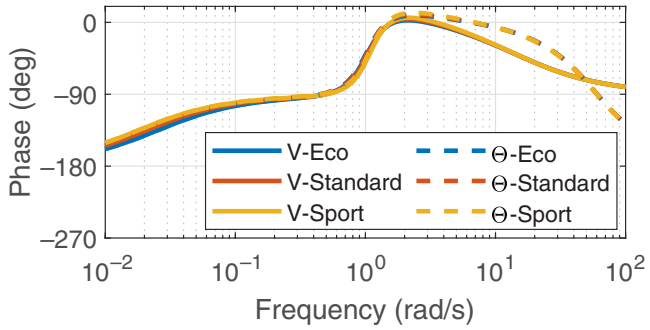

Fig. 16. Phase frequency response of longitudinal input to pitch attitude ($\angle\theta/V_{1c}$ and $\angle\theta/\Theta_{1c,cmd}$).

Table 7. Yaw stability and control derivatives

Trim Point	N_r	N_Ω	N_V	T_Θ
Eco (1050 RPM)	−0.050	−0.12	0.11	−6.1
Standard (1200 RPM)	−0.041	−0.12	0.11	−8.4
Sport (1350 RPM)	−0.036	−0.12	0.11	−10.0

less sensitive to rotor speed (M_Ω, Fig. 14), but more sensitive to root pitch (M_Θ, Fig. 15). At very low frequency, this difference is exaggerated by the change in the zero location when considering RPM control (Fig. 14) but reduced when considering pitch control (Fig. 15). The phase response for either control type remains similar regardless of trim point up to the frequency of at which the actuator dynamics begin to affect the response (Fig. 16). Like in heave, the response from the voltage input lags that from pitch input due to differences in actuator bandwidth.

Linearized yaw dynamics. As mentioned previously during the derivation of input scaling, the yaw dynamics are fundamentally different from the other axes in that the response depends on the motor reaction torque, rather than the rotor thrust. Since differential voltage (V_d) has a direct effect on the yaw acceleration and an indirect effect via Ω_d, there is a zero in the transfer function r/V_d in addition to the expected two poles from rigid body and motor dynamics.

$$\frac{r}{V_d} \approx \frac{N_V}{(s-N_r)} \frac{(s - T_\Omega + T_V N_\Omega / N_V)}{(s - T_\Omega)} \tag{22}$$

In the absence of motor speed feedback, the blade pitch has no direct effect on the motor torque and no immediate impact on the yaw acceleration. It does, however, influence the motor speed via aerodynamic torque. This affects the back electromotive force produced by the motor, changing the motor current and reaction torque. Thus, the transfer function r/Θ_d is an overdamped second-order system,

$$\frac{r}{\Theta_{d,cmd}} \approx \underbrace{\frac{N_\Omega}{(s-N_r)} \frac{T_\Theta}{(s-T_\Omega)}}_{r/\Theta_d} \underbrace{G_\Theta}_{\Theta_d/\Theta_{d,cmd}} \tag{23}$$

The stability and control derivatives for the yaw axis are listed in Table 7. Again, the values T_Ω and T_V are not repeated as the motors are assumed to be identical. For higher trim rotor speed, the yaw rate damping (N_r) becomes smaller, while the motor speed is more sensitive to changes in blade pitch as rotor speed increases.

The magnitude frequency responses for RPM and pitch control of the yaw axis are shown in Figs. 17 and 18, respectively. Considering RPM control, the frequency response magnitude is not significantly impacted by the operating point, as the motor dynamics are not very sensitive to their operating state. With pitch control, the gain is higher for higher trim rotor speed due to the increase in sensitivity of motor torque to collective pitch, T_Θ.

The phase frequency response for RPM- and pitch-control is shown in Fig. 19. As in the other axes, the choice of trim point does not substantially affect the phase response, and both control strategies are dominated by the rigid body dynamics at very low frequency. However, unlike the

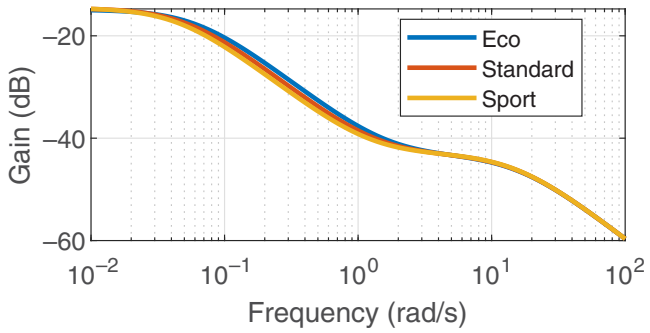

Fig. 17. Magnitude frequency response of motor voltage input to yaw rate ($|r/V_d|$).

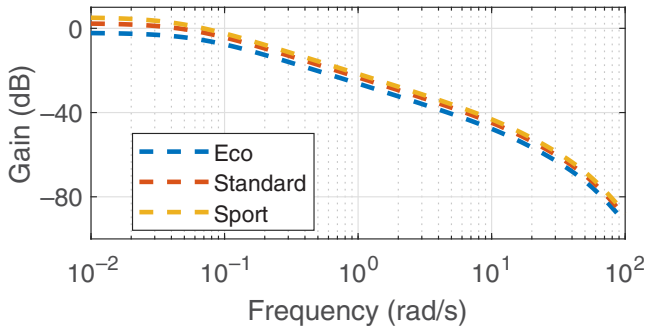

Fig. 18. Magnitude frequency response of blade pitch input to yaw rate ($|r/\Theta_{d,cmd}|$).

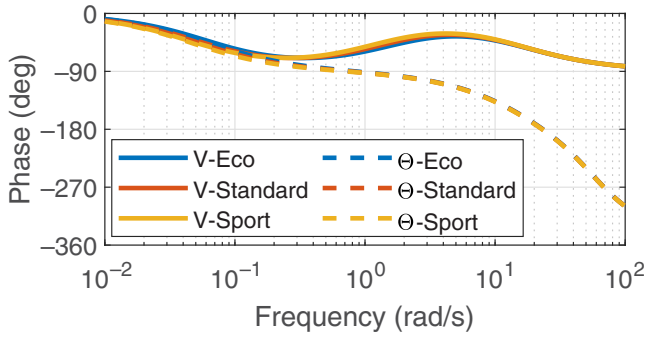

Fig. 19. Phase frequency response of differential input to yaw rate ($\angle r/V_d$ and $\angle r/\Theta_{d,cmd}$).

thrust-dominated axes, there is phase lead in the mid- to high-frequency range when using RPM control, the opposite that was observed with the other axes. This is primarily due to the direct effect that voltage has on yaw rate, represented by the zero in Eq. (22), which also prevents additional phase roll-off at high frequency.

Pure RPM and pitch control

Before hybrid control is considered, the aircraft response is examined with pure RPM control or pure pitch control through a series of time domain simulations of the system linearized about the three hover trim points. These simulations are presented in order to examine the transient response of the aircraft with controllers designed to meet 70% of the maximum achievable design margin.

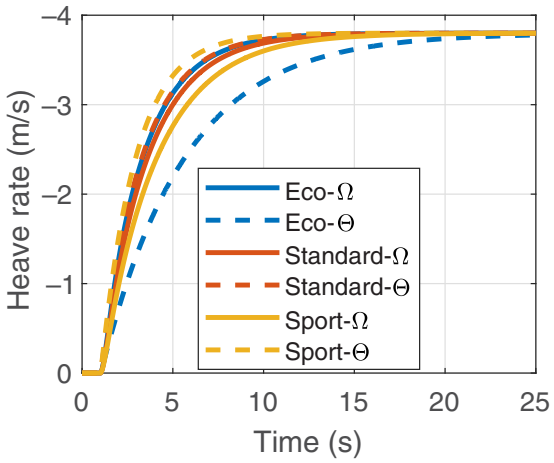

Fig. 20. Heave step response with pure RPM or pitch control.

Table 8. Design margin optimization on the heave axis

Mode	Design Margin (%)	Limit
Eco - Ω	100	OLOP (disturbance)
Eco - Θ	0	Maximum blade pitch
Standard - Ω	70	Maximum current
Standard - Θ	110	OLOP (disturbance)
Sport - Ω	40	Maximum current
Sport - Θ	150	OLOP (disturbance)

Heave response. The first simulation is a heave rate step response. The design margins achieved by each trim point and control strategy are listed in Table 8, with heave handling qualities metrics listed in the Appendix for each case. No design margin is implemented on the Eco trim point with pitch control since this operating point was defined using the minimum stall margin that allowed satisfactory heave handling qualities. With increasing trim rotor speed, the design margin for pitch control increases as a result of the increased stall margin as well as the increased sensitivity to changes in pitch (Table 5).

The design margin with RPM control shows the opposite trend as pitch control, with decreasing design margin at higher trim rotor speeds as a result of increased trim current. This trend is also reflected in the decreasing sensitivity of heave rate to changes in rotor speed seen in Table 5. It is worth noting that the DMO reaches the current limit around a similar design margin as the OLOP specification reached the limit of satisfactory values. The rate limit imposed for the OLOP specification restricts the rotor acceleration based on the same maximum current limit, and this suggests that the OLOP specification boundaries may be sufficient to avoid saturation of motor current during a step response when using rotor speed control.

The aircraft is commanded to climb rate of 3.8 m/s (760 ft/min) at time $t = 1$ s, and responses are shown in Fig. 20. The differing rise times seen in Fig. 20 demonstrate the increased responsiveness that comes with higher design margin. For example, Eco mode with pitch control and Standard with RPM control have similar design margins and, as a result, the heave responses are nearly identical, while Sport mode with pitch control achieves the highest design margin and the fastest heave response (lowest setting time). Conversely, with zero design margin, the heave response of Eco mode with pitch control represents the slowest allowable heave response to qualify as Level 1 (based on requirements from Ref. 6).

The collective rotor speed and blade pitch during the heave rate step response are shown in Fig. 21. The feedback control on the rotor speed

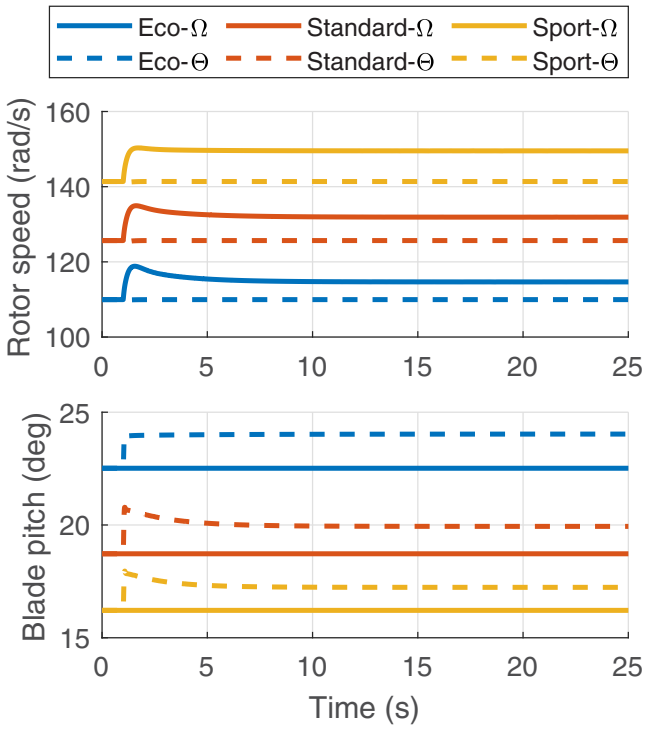

Fig. 21. Blade pitch and rotor speed during heave response with pure RPM or pitch control.

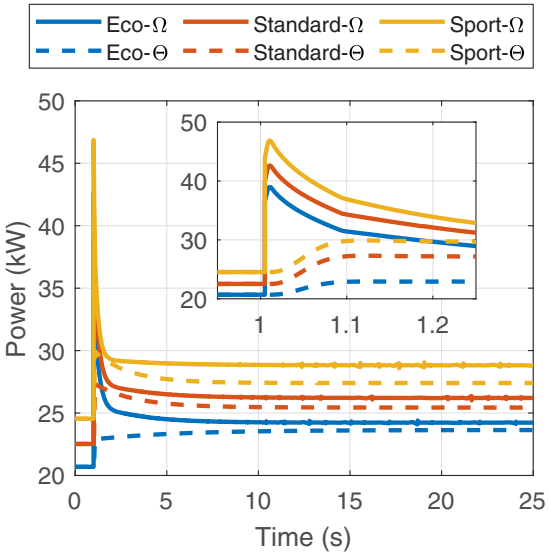

Fig. 22. Single motor power during heave response with pure RPM or blade pitch control.

keeps it at the trim value when using pitch control (solid lines), while an increase in blade pitch produces the additional thrust to accelerate the aircraft. When using RPM control (dashed lines), the rotor speed changes to produce more thrust, while the root pitch remains at the trim value.

The power to a single motor during the heave simulation is shown in Fig. 22. As expected, RPM control requires significant spikes in power (and current) in order to overcome rotor inertia and quickly produce the change in thrust needed to accelerate the aircraft upward. These spikes are not seen in the pitch-control cases since this control strategy only needs to overcome aerodynamic torque. This suggests that pitch control

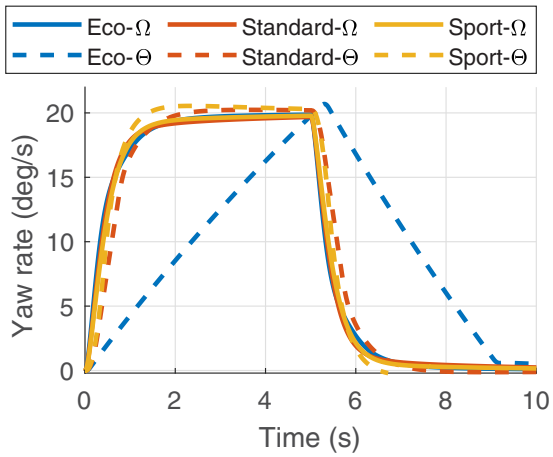

Fig. 23. Yaw response with pure RPM or pitch control.

Table 9. Design margin optimization on the yaw axis

Mode	Design Margin (%)	Limit
Eco - Ω	70	OLOP (disturbance)
Eco - Θ	–	Maximum blade pitch
Standard - Ω	60	OLOP (disturbance)
Standard - Θ	–	Maximum blade pitch
Sport - Ω	40	OLOP (disturbance)
Sport - Θ	40	Maximum blade pitch

is better for thrust-driven maneuvers since it requires smaller bursts of power/current to produce changes in thrust. At lower trim rotor speed (Eco Mode), pitch control is not able to achieve as fast a response as RPM control, since this mode trades stall margin and responsiveness for reduced power. The reverse is true for Sport mode, which has higher trim power but also the fastest response.

Yaw response. Table 9 shows the design margin achieved in the yaw axis for each trim point and control strategy. Due to the low sensitivity of rotor torque to pitch input, pitch control was typically inferior to RPM control, since the pitch actuators tended to reach their maximum positions during yaw commands. This was not captured during the control design phase due to the lack of actuator position constraints in Table 3 but could be captured during the optimization by including a time domain specification on the maximum achievable yaw acceleration with pitch control. Eco and Standard mode with pitch control were unable to meet Level 1 yaw handling qualities requirements without actuator saturation, and yaw handling qualities metrics are listed in the Appendix for each case.

A 20-deg/s command in yaw rate is held for 5 s, with responses shown in Fig. 23. With the exception of pitch control in Eco mode, similar performance is shown at all trim points and control strategies. With pitch control in Eco mode, however, the pitch actuator position saturates at the maximum blade pitch imposed to avoid stall. As a result, the maximum yaw acceleration is severely limited, preventing the system from following the first-order command model. Thus, it can be concluded that exclusive pitch control is not feasible for this configuration in yaw. Saturation also occurs for Standard mode with pitch control, though the effect is less severe.

Figure 24 shows the rotor speed and blade pitch during the yaw step. Due to the fact that the motor dynamics are insensitive to the trim condition, the change in rotor speed during the yaw step is identical for all three trim points. The pitch inputs, however, are characterized by

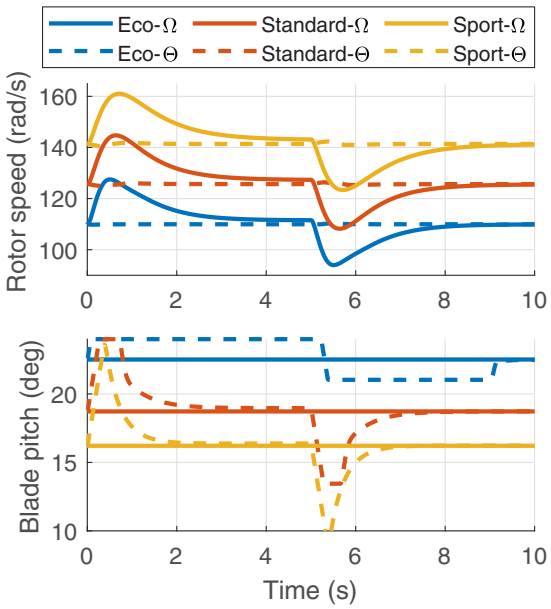

Fig. 24. Rotor speed and blade pitch during yaw response with pure RPM or pitch control.

both rate and position saturation, even in Sport mode. Due to this, and the lack of substantial performance improvements, the use of collective pitch control is not recommended when reaction torque is used to control the vehicle.

Trim in hot/high conditions

The use of hybrid control provides benefits over RPM- or pitch-control alone. With an electric drive-train, the aircraft does not have the reduction in motor power associated with traditional turbine engines in hot/high conditions. The redundancy of trim control actuators that comes with hybrid control allows for additional considerations when trimming in hot or high conditions.

For each of the trim points (Eco, Standard, and Sport), hover trim is simulated at increasing altitude for ISA+20 conditions (Fig. 25). Both the rotor speed and root pitch trim control strategies are considered. When trimming with collective root pitch, the ceiling is limited by the maximum deflection of the pitch actuator (24°). The ceiling varies at the different trim points based on the available stall margin of the pitch actuators. When trimming rotor speed (as is done with hybrid control) the ceiling is limited by an imposed maximum total continuous power constraint of 160 hp (120 kW). Here, starting at a higher trim power in hover leads to less power margin available to achieve higher ceiling.

Table 10. Ceiling with different trim strategies (ft)

Mode	Absolute Ceiling	Service Ceiling
Eco - Ω	24,900	24,000
Eco - Θ	910	590
Standard - Ω	19,400	18,500
Standard - Θ	10,300	10,000
Sport - Ω	13,600	12,600
Sport - Θ	18,300	18,100

The service ceiling is found by considering the maximum altitude at which the aircraft can achieve a 100 ft/min (0.5 m/s) climb rate, as defined by Ref. 17. The absolute and service ceilings for each control strategy are listed in Table 10. Trimming with rotor speed (as with hybrid control) allows higher ceiling, except for Sport mode, without consuming any stall margin for maneuvers.

Thus, hybrid control is beneficial in hot/high conditions, as it allows the aircraft to trim with rotor speed while maintaining stall margin available for maneuvers, though this comes with a trade-off of greater power consumption.

Trim in axial climb

Moving on from hover, analysis of the use of hybrid control can also be performed in axial climb. Like in hover, with the redundancy of control actuators, both the collective rotor speed and collective root pitch can be used to trim the vehicle in climb.

Starting from the Standard mode trim point, three trim strategies are considered with increasing climb rate (Fig. 26). Either the root pitch or rotor speed can be fixed (as was considered for control in hover), while the other control input is used for trim. Using pitch control to trim in axial climb is the most power-efficient option but will consume stall margin. Another option is to fix the effective angle of attack (α_{75}) which will maintain the hover stall margin in climb. This option increases both the rotor speed and root pitch to trim in climb and requires only marginally more power than when trimming with root pitch alone.

Scheduling of pitch input. Effective stall margin (and by extension, maneuverability with hybrid control) can be maintained by scheduling the trim root pitch with commanded climb rate. From Fig. 26, the change

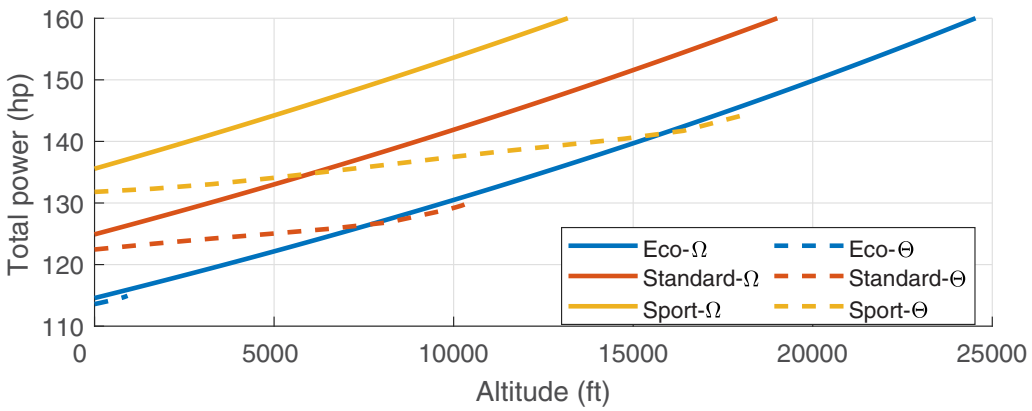

Fig. 25. Power with increasing altitude (ISA+20).

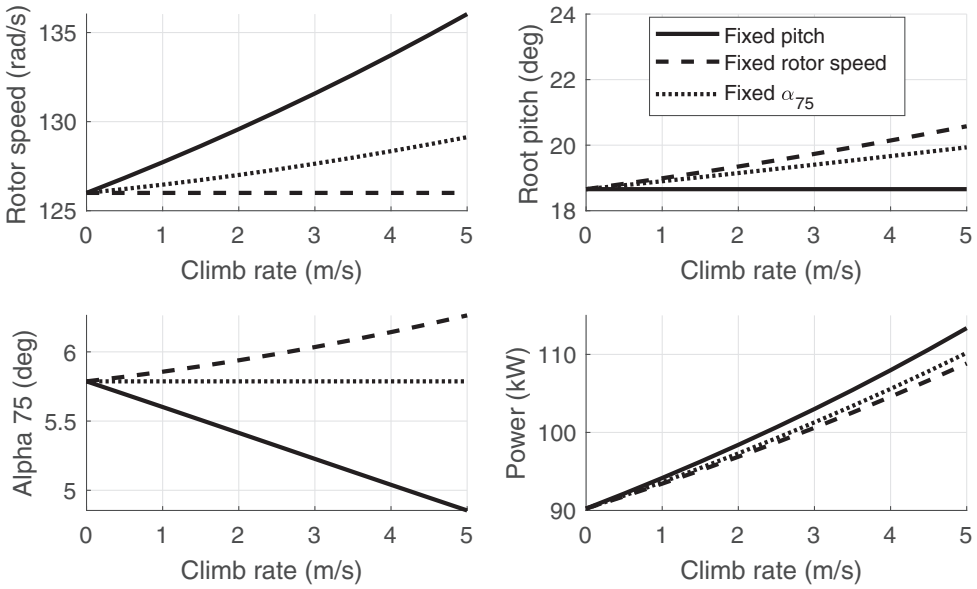

Fig. 26. Trim in axial climb.

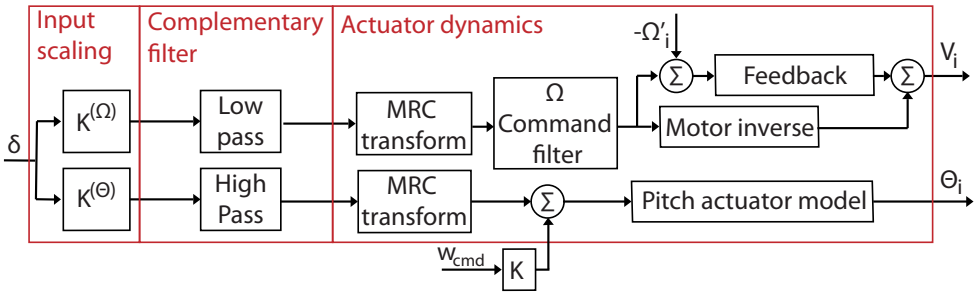

Fig. 27. Hybrid control architecture with additional feedforward compensation.

in root pitch needed to maintain the effective angle of attack is approximated as being linear with the climb velocity (heave rate in axial climb conditions):

$$\Delta\Theta_0 = K w_{cmd} = -0.2512 w_{cmd} \tag{24}$$

In order to schedule the root pitch with climb rate, an additional feedforward path is added to the pitch path of the hybrid control mixer (Fig. 27). The addition of this path affects the model following of the heave axis, but the model inverse approximation is adjusted in order to account for the additional feedforward compensation.

Using the input scaling found in Table 2 and linearized heave dynamics neglecting motor dynamics (Eq. (9)), the heave response for acceleration input δ can be represented in the frequency domain as

$$w \approx \frac{\delta}{Z_\Omega}\left(\frac{s}{s+\alpha}\right)\frac{Z_\Omega}{s-Z_w} + \left(\frac{\delta}{Z_\Theta}\left(\frac{\alpha}{s+\alpha}\right) + K w_{cmd}\right)\frac{Z_\Theta}{s-Z_w} \tag{25}$$

The sum of the high- and low-pass filter dynamics can be treated as unity gain, and the input scaling is designed to cancel out additional differences in gain between the RPM- and pitch-control paths, so the expression for heave response can be simplified:

$$w \approx \frac{\delta + Z_\theta K w_{cmd}}{s - Z_w} \tag{26}$$

With the assumption that $w = w_{cmd}$ (as is true for good model following), the approximation of input δ to output w is represented by a pole:

$$w = w_{cmd} \implies \frac{w}{\delta} \approx \frac{1}{s - Z_w - K Z_\Theta}. \tag{27}$$

Thus, the additional feedforward compensation used to schedule root pitch with climb rate shifts the location of the effective heave pole by $K Z_\Theta$. The inverse heave model approximation is updated to reflect this shift in pole location and improve model following with the scheduling of collective root pitch.

Hybrid control compared to pitch control

Thus far, simulations with different trim points and pure RPM or pitch control have been considered. It has been shown that pitch control is more effective for the thrust-driven roll, pitch, and heave axes, while RPM control is better for the torque-driven yaw axis. Now, pitch control will be compared to hybrid control for thrust-driven responses. A cutoff frequency of 1 rad/s is chosen for the complementary filter of the hybrid controller. The feedback controllers optimized for the purely pitch-based controllers are applied to the hybrid controller since the short-term responses (on which the specifications in Table 3 are based) are governed by the pitch actuators.

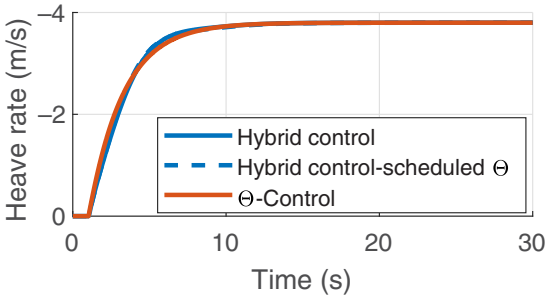

Fig. 28. Heave response with hybrid control.

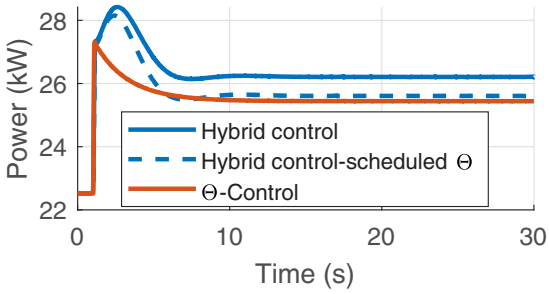

Fig. 29. Single motor power during heave response with hybrid control.

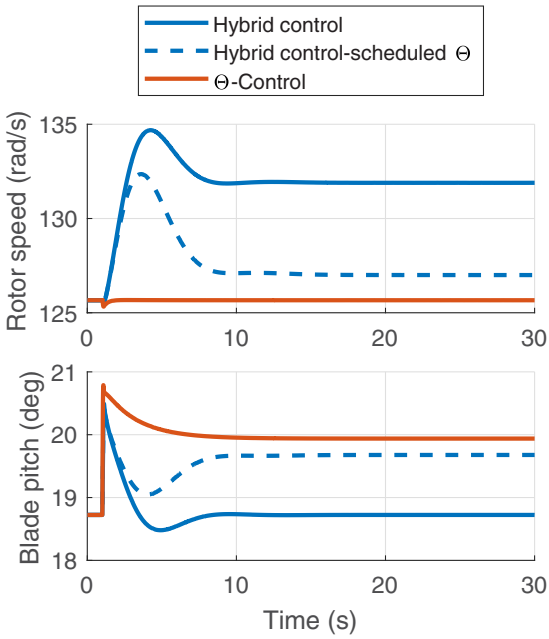

Fig. 30. Rotor speed and blade pitch during heave response with hybrid control.

Heave rate step. A step in heave rate is simulated on the aircraft model linearized about the Standard trim point with hybrid control (Fig. 28). With a design margin of 1.4, the heave response is the same with the hybrid (with and without pitch scheduling) and pitch controllers, as expected.

The power consumption during the heave simulation with hybrid control is shown in Fig. 29. The initial spike in power seen with RPM control (Fig. 22) becomes less severe as the pitch actuator is used to generate the initial thrust increment to enter climb and less current is

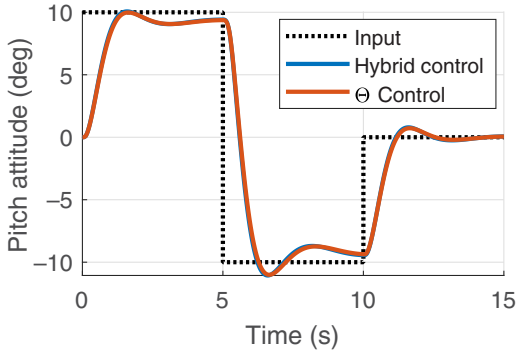

Fig. 31. Response to pitch doublet input with pitch and hybrid control.

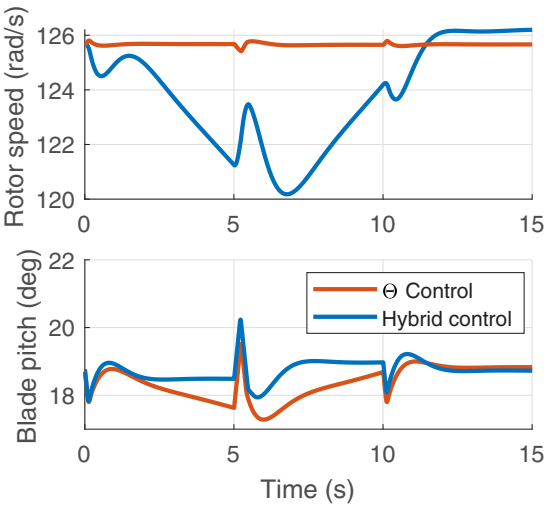

Fig. 32. Rotor 1 speed and blade pitch during pitch doublet.

needed when the rotor is allowed to accelerate more slowly. With $\alpha = 1$ rad/s, the initial heave acceleration requires slightly more motor power (4%) than pitch control, but this effect could be reduced by reducing α and allowing the rotor speed to change more slowly. As the rotor speed settles to a higher trim value, the power remains higher with hybrid control as a result of higher voltage needed to maintain the rotor speed. This implies that pure pitch control is more power efficient for climb, as was found in Ref. 7 and Fig. 26.

The trim power in climb is reduced by scheduling the blade pitch with climb rate, essentially trading the additional stall margin gained by entering axial climb for a reduction in power. With this scheduling, the hybrid controller settles closer to the trim value of the inputs seen with pure pitch control, rather than trimming with only the rotor speed (Fig. 30).

Pitch attitude doublet. The pitch response with hybrid control is analyzed using a doublet input in pitch attitude simulated using the linear model, again in Standard mode. This input commands the aircraft to pitch 10° nose up for 5 s and then 10° nose down for 5 s before returning to hover. This produces the maximum change in commanded pitch attitude of 20°. The feedback control gains and command filters corresponding to the design-margin-optimized pitch-based controller are applied to both the hybrid and pitch controllers.

The aircraft response to the pitch doublet is the same regardless of control type (Fig. 31). The rotor speed and blade pitch of rotor 1 during

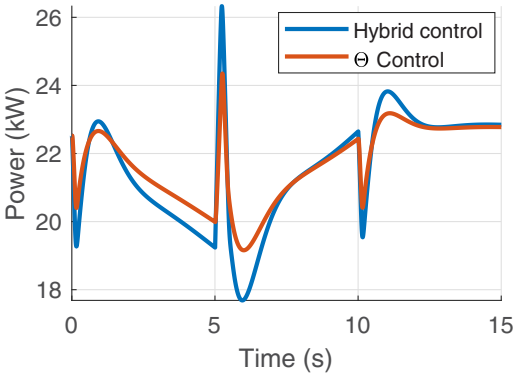

Fig. 33. Rotor 1 power during pitch doublet.

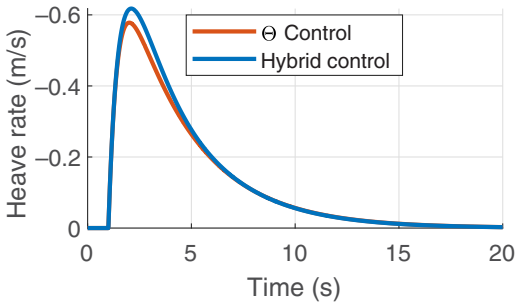

Fig. 34. Heave rate with payload drop-off.

the doublet are plotted in Fig. 32. Small changes in rotor speed are visible with pitch control before the RPM feedback brings the rotor speed back to the trim value. Due to the ACAH control type, the aircraft translates slowly at the end of the simulation (no feedback on velocity is present), resulting the in rotor speed settling to a slightly different trim value when using hybrid control, and the blade pitch to be slightly higher when using pitch control.

The power to rotor 1 during the pitch doublet is shown in Fig. 33. The pitch and hybrid control require similar small peaks in power to each rotor, though the total power will remain close to the trim value.

Hybrid control for payload change. Further benefits of hybrid control for heave control can be demonstrated by considering changing trim conditions in simulations of the nonlinear model with either pure pitch or hybrid ($\alpha = 1$ rad/s) control. Consider a case of payload drop-off where the weight of the vehicle is instantaneously reduced by 80 kg (15% gross weight) at $t = 1$ s (e.g., releasing a slung load in hover). As shown in Fig. 34, this sudden reduction in weight causes the aircraft to initially accelerate upward before returning to hover. The aircraft response is essentially the same for either control type.

The rotor speed and collective pitch inputs during the payload drop-off are shown in Fig. 35. With pitch control, the collective blade pitch initially decreases in order to reduce the thrust. It then stays at a lower value as a new trim condition with lower thrust is reached. With hybrid control, the collective blade pitch initially decreases in order to quickly reduce thrust, but then returns to its nominal value as the rotor speed slows to trim the aircraft.

The fact that the aircraft becomes 80 kg lighter naturally reduces the power required to hover, regardless of control strategy (Fig. 36). However, the power reduction is 24.3% greater when hybrid control is used instead of pure pitch control, resulting in a 5.0% lower trim power at the reduced aircraft gross weight. The additional power consumed by the pitch-based controller does have a potential benefit though. Because

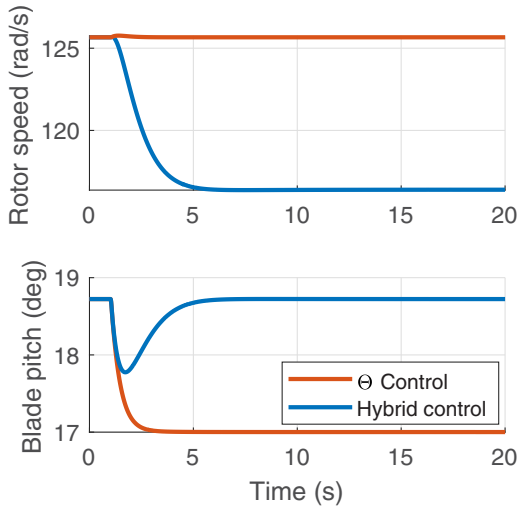

Fig. 35. Collective control inputs with payload drop-off.

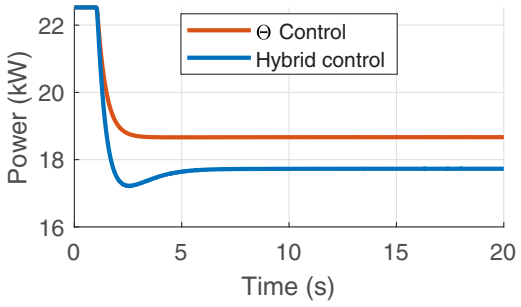

Fig. 36. Power with payload drop-off.

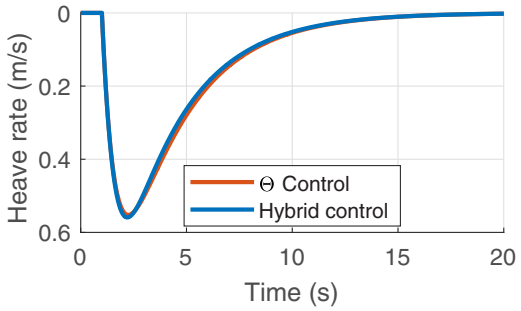

Fig. 37. Heave rate with payload pickup.

the rotor is operating at a higher speed and lower collective pitch, it has additional stall margin, relative to the hybrid controller, but this excess stall margin does not affect the command filters or feedback gains, so no piloted or disturbance rejection bandwidth is gained. Thus, the hybrid controller can afford to trade the excess stall margin for reduced power consumption.

Converse to the payload drop-off, if additional payload is acquired the aircraft has the opposite response (Fig. 37). The hybrid controller increases the power by a greater margin than the purely pitch-based controller, as shown in Fig. 38. However, the lower power consumed using the pitch-based controller comes at the cost of stall margin, which may result in saturation of the pitch actuators if maneuvers are executed while carrying the extra payload. The hybrid controller mitigates this risk by increasing rotor speed and consuming more power to maintain a certain stall margin in hover (Fig. 39).

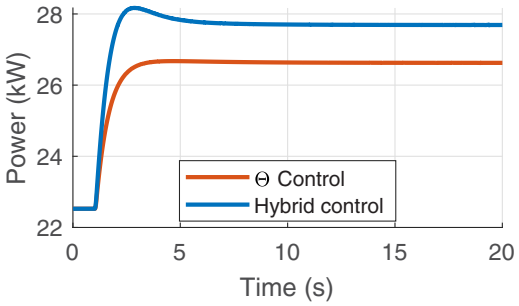

Fig. 38. Power with payload pickup.

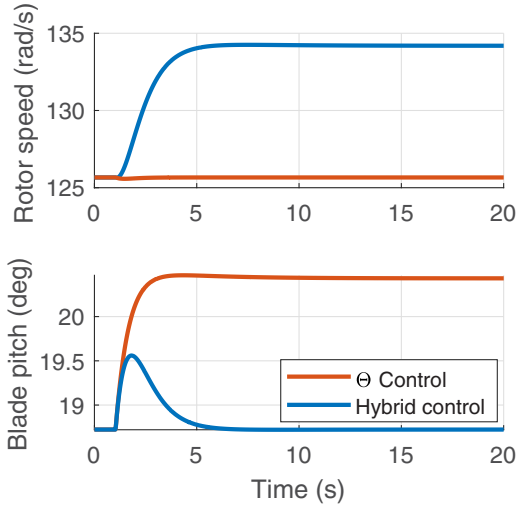

Fig. 39. Collective control inputs with payload pickup.

Discussion

A UAM-scale quadcopter with both variable rotor speed and variable collective pitch on each rotor was simulated in hover. Through hover trim analysis, it was found that having both motor voltage and blade pitch available as control inputs allows a choice of trim point. Generally speaking, operation at lower RPM was found to be associated with lower power consumption but also reduced stall margin. The choice of trim point was shown to affect the dynamics of the aircraft. Analyzing the hover dynamics at three different trim points showed that higher trim rotor speed increased the sensitivity of thrust-driven responses to changes in collective pitch but reduced sensitivity to RPM changes.

The observed differences in dynamics, as well as the differences in stall margin, affect the achievable design margins when considering pure RPM or pitch control at the different trim points. Similar to the trends in control derivatives, the heave design margin increases with higher trim rotor speed when using pitch control but decreases with RPM control. It was also observed that the use of pitch control for heave acceleration eliminates the power spikes associated with the initial acceleration of the rotors.

Thus, having both variable rotor speed and variable blade pitch allows the hybrid control aircraft to trade increased power for increased agility by changing trim point. A single aircraft could be adapted based on the maneuverability and endurance requirements of a mission. For example, the aircraft may take advantage of Eco mode for a slow, predictable mission (i.e., hovering in place with minimal turbulence) that requires the aircraft to be in the air for a longer amount of time without recharging. However, the same aircraft could be switched to Sport mode for a mission that requires greater agility and disturbance rejection capabilities but with shorter flight time.

Two key differences between the torque-driven yaw dynamics and thrust-driven axes were identified. First, the blade pitch inputs have no direct effect on the yaw acceleration. Rather, they influence the yaw rate indirectly through the motor dynamics. Second, changes in motor voltage have both a direct effect on yaw acceleration and an indirect effect via rotor acceleration. Thus, the motor dynamics can be represented by a pole-zero pair, resulting in lead–lag behavior, rather than a simple lag, as was observed for the thrust-dominated axes.

When considering pure RPM or pitch control for the torque-driven yaw axis, pitch control (and by extension, hybrid control) provided no advantage over RPM control for the uncanted rotors considered in this study. With pure pitch control, two of the trim points (Eco and Standard modes) were unable to provide satisfactory yaw response without pitch actuator saturation. Thus, it is suggested that RPM control be used for control of the yaw axis, assuming un-canted rotors.

Trim was also considered in axial climb. The redundancy of controls allowed for the scheduling of the blade pitch to maintain the effective stall margin during climb, allowing the aircraft to operate at lower trim power in climb than when trimming with RPM alone. The heave inverse model was updated to reflect the additional feedforward compensation on the blade pitch, and improve model following.

The use of a complementary filter for hybrid control mixing routes high-frequency (maneuver) input content to the pitch actuator and low-frequency (trim) input content to rotor speed commands. For the model inversion, the equivalent delay is found to be driven by the pitch actuator and can be fixed to a constant value as long as $\alpha \leq 1/\tau_\Omega$. Through consideration of different complementary filter cutoff frequencies and motor time constants, it was found that the motor time constant should be limited to a maximum of $0.1/\alpha$ in order to avoid giving commands to the motors that they cannot adequately follow. When using primarily pitch control for maneuvers, the value of the motor time constant time can be fixed to $0.1/\alpha$ with no impact on the vehicle dynamics, as the low-pass filter dominates over the closed-loop motor dynamics. This eliminates a design parameter, simplifying the optimization of the control laws.

Using a complementary filter for hybrid control mixing, the aircraft is able to combine the benefits of pitch control for maneuvers with the trim benefits of RPM control in steady-state operation. Through comparison of hybrid control to pitch control, it was shown that hybrid control of the heave axis can provide the same response with similar transient power while recovering stall margin in trim.

The benefits of hybrid control are further demonstrated through consideration of trim in hot/high/heavy conditions. Utilizing the rotor speed to trim in these conditions allowed the aircraft to maintain the original stall margin of the pitch actuators for maneuvers. From simulation of a drop-off of payload weight, the hybrid control scheme provided a 5% reduction in trim power compared to pitch control. Conversely, when the payload was picked up, hybrid control required 5% higher trim power compared to pitch control, but maintained stall margin available for maneuvers.

Conclusions

Several key conclusions are drawn from the examination of the hover dynamics and flight control of the UAM-scale quadcopter with hybrid RPM/pitch control presented in this study:

1) By operating at higher trim rotor speed and lower blade pitch in hover, increased trim power can be traded for greater maneuverability as a result of increased stall margin and sensitivity to pitch inputs when considering thrust-driven responses.

2) The torque-driven yaw dynamics differ from the other axes, and hybrid control offers no benefit over RPM control for yaw maneuvers.

3) The use of a complementary filter routes high-frequency input content to the pitch actuators and low-frequency input content to changes in rotor speeds, allowing the aircraft to utilize the faster response of the pitch actuators for maneuvers while still gaining the benefits of utilizing changes in rotor speeds to trim.

4) For thrust-driven maneuvers, hybrid control eliminates the spikes in power needed to overcome rotor inertia when using RPM control alone by quickly producing changes in thrust with blade pitch actuators.

5) Hybrid control allows the aircraft to maintain maneuverability when operating in hot/high/heavy conditions by trimming with the rotor speed and maintaining the original stall margin.

Acknowledgments

This work is carried out at Rensselaer Polytechnic Institute under the Army/Navy/NASA Vertical Lift Research Center of Excellence (VLRCOE) Program, grant number W911W61120012, with Dr. Mahendra Bhagwat as Technical Monitor. The authors would like to acknowledge the Army Combat Capabilities Development Command for sponsoring Ms. Ariel Walter through the Science Mathematics and Research Transformation (SMART) Scholarship Program.

Appendix

Table A1. Heave handling qualities

	Eco		Standard		Sport		
	RPM	Pitch	RPM	Pitch	RPM	Pitch	Level 1
Design margin	1.0	0	0.7	1.1	0.4	1.5	0
Phase margin (deg)	72	89	75	86	82	85	45
Gain margin (dB)	36	34	38	30	40	28	6
Crossover (rad/s)	1.7	1.0	1.6	1.7	1.3	1.9	1.0
DRB (rad/s)	1.5	1.0	1.4	1.6	1.2	1.8	1.0
DRP (dB)	1.5	0.2	1.4	0.4	1.0	0.4	5.0
Heave mode (rad/s)	0.40	0.20	0.34	0.42	0.28	0.5	0.2
Heave delay (s)	0.12	0.03	0.12	0.03	0.11	0.03	0.2
Model following	50	4.0	50	5.8	50	5.0	50
OLOP phase, pilot (deg)	[a]	−102	[a]	−98	[a]	−99	[b]
OLOP Mag, Pilot (dB)	[a]	−15	[a]	−7.3	[a]	−7.7	[b]
OLOP phase, dist (deg)	−105	−91	−102	−94	-98	−94	[b]
OLOP mag, dist (dB)	3.0	0.9	2.1	4.5	0.3	4.1	[b]
Maximum current (% Hover)	178	113	179	128	182	118	200
Maximum pitch (deg)	[c]	23.9	[c]	21.6	[c]	19.0	24.0
RMS, pilot	1.04	0.49	0.38	0.43	0.30	0.48	1.5
RMS, dist	0.98	0.51	0.35	0.35	0.27	0.37	1.5

[a]No open-loop-onsite-point in the frequency range.
[b]OLOP boundaries are shown in Fig. 8.
[c]Fixed pitch at hover value (Table 4).

Table A2. Yaw handling qualities

	Eco		Standard		Sport		
	RPM	Pitch	RPM	Pitch	RPM	Pitch	Level 1
Design margin	0.7	0	0.6	0	0.4	0.4	0
Phase margin (deg)	51	56	70	66	71	76	45
Gain margin (dB)	24	10	33	13	35	18	6
Crossover (rad/s)	6.3	10	2.4	7.3	2.1	3.6	1.0
DRB (rad/s)	4.3	6.9	1.3	5.4	1.6	2.9	1.0
DRP (dB)	3.4	0.3	1.5	1.3	1.4	1.3	5.0
Bandwidth (rad/s)	2.0	1.4	1.9	1.4	1.8	1.9	1.4
Phase delay (s)	0.06	0.08	0.06	0.07	0.06	0.04	0.2
Model following	50	50	50	50	31	50	50
OLOP phase, pilot (deg)	−133	−99.6[d]	–	−100[d]	[a]	−102	[b]
OLOP mag, pilot (dB)	1.3	13.2[d]	–	8.0[d]	[a]	2.2	[b]
OLOP phase, dist (deg)	−132	−101[d]	–	−102[d]	[a]	−105	[b]
OLOP mag, dist (dB)	1.7	11.1[d]	–	6.7[d]	[a]	−1.2	[b]
Maximum current (% Hover)	184	109	178	153	174	190	200
Maximum pitch (deg)	[c]	24.0[d]	[c]	24.0[d]	[c]	23.6	24.0
RMS, pilot	0.40	0.39	0.15	0.15	0.15	0.23	1.5
RMS, dist	0.16	0.16	0.06	0.06	0.06	0.09	1.5

[a]No open-loop-onsite-point in the frequency range.
[b]OLOP boundaries are shown in Fig. 8.
[c]Fixed pitch at hover value (Table 4).
[d]Unable to meet Level 1.

References

[1]Walter, A., McKay, M., Niemiec, R., Gandhi, F., and Ivler, C., "Hover Handling Qualities of Fixed-Pitch, Variable-RPM Quadcopters of Increasing Size," *Journal of the American Helicopter Society*, **67**, 042010 (2022), pp. 1–18. DOI: 10.4050/JAHS.67.042010.

[2]Malpica, C., and Withrow-Maser, S., "Handling Qualities Analysis of Blade Pitch and Rotor Speed Controlled eVTOL Quadrotor Concepts for Urban Air Mobility," Proceedings of the Vertical Flight Society International Powered Lift Conference, San Jose, CA, January 21–23, 2020.

[3]Niemiec, R., Gandhi, F., Lopez, M., and Tischler, M., "System Identification and Handling Qualities Predictions of an eVTOL Urban Air Mobility Aircraft Using Modern Flight Control Methods," Proceedings of the 76th Annual Forum of the Vertical Flight Society, Virtual, October 6–8, 2020.

[4]Walter, A., McKay, M., Niemiec, R., Gandhi, F., Hamilton, C., and Jaran, C., "An Assessment of Heave Response Dynamics for Electrically Driven Rotors of Increasing Diameter," Proceedings of the Autonomous VTOL Technical Meeting & eVTOL Symposium, Mesa, AZ, January 9–11, 2019.

[5]Theron, J. P., Horn, J., Wachpress, D., and Enciu, J., "Nonlinear Dynamic Inversion Control for Urban Air Mobility with Distributed Electric Propulsion," Proceedings of the VFS International 76th Annual Forum, Virtual, October 6–8, 2020.

[6]"Aeronautical Design Standard, Performance Specification, Handling Qualities Requirements for Military Rotorcraft," ADS-33E-PRF, 2000.

[7]McKay, M., Niemiec, R., and Gandhi, F., "Performance Comparison of Quadctopers with Variable-RPM and Variable-Pitch Rotors," *Journal of the American Helicopter Society*, Vol. 64, (4), 2019, pp. 1–14. DOI: 4050/JAHS 64.042006.

[8]Niemiec, R., and Gandhi, F., "Development and Validation of the Rensselaer Multicopter Analysis Code (RMAC): A Physics-Based Comprehensive Modeling Tool," Proceedings of the 75th Annual Forum of the Vertical Flight Society, Philadelphia, PA, May 13–16, 2019.

[9]Peters, D., Boyd, D., and He, C., "Finite-State Induced-Flow Model for Rotors in Hover and Forward Flight," *Journal of the American Helicopter Society*, Vol. 34, (4), 1989, pp. 5–17. DOI: 10.4050/JAHS.34.5.

[10]Niemiec, R., "Development and Application of a Medium-Fidelity Analysis Code for Multicopter Aerodynamics and Flight Mechanics," Ph.D. Thesis, Rensselaer Polytechnic Institute, Troy, NY, 2018.

[11]Niemiec, R., and Gandhi, F., "Multi-rotor Coordinate Transform for Orthogonal Primary and Redundant Control Modes for Regular Hexacopters and Octocopters," Proceedings of the 42nd European Rotorcraft Forum, Lille, France, September 5–8, 2016.

[12]Tischler, M., Berger, T., Ivler, C., Mansur, M., Cheung, K., and Soong, J., *Practical Methods for Aircraft and Rotorcraft Flight Control Design: An Optimization-Based Approach*, AIAA Education Series, AIAA, Reston, VA, 2017.

[13]Ballin, M., and Dalang-Secretan, M.-A., "Validation of the Dynamic Response of a Blade-Element UH-60 Simulation Model in Hovering Flight," *Journal of the American Helicopter Society*, Vol. 36, (6), 1990, pp. 77–88. DOI: 10.4050/JAHS.36.77.

[14]Tischler, M., and Remple, R., *Aircraft and Rotorcraft System Identification*, AIAA Education Series, AIAA, Reston, VA, 2012.

[15]Berger, T., Ivler, C., Berrios, M., Tischler, M., and Miller, D., "Disturbance Rejection Handling-Qualities Criteria for Rotorcraft," Proceedings of the 72nd Annual Forum of the American Helicopter Society, West Palm Beach, FL, May 16–19, 2016.

[16]Duda, H., "Flight Control System Design Considering Rate Saturation," *Aerospace Science and Technology*, Vol. 2, (4), 1998, pp. 265–275. DOI: 10.1016/S1270-9638(98)80004-7.

[17]United States Department of Transportation, Federal Aviation Administration, Airman Testing Standards Branch, *Pilot's Handbook of Aeronautical Knowledge*, FAA-H-8083-25B, Oklahoma City, OK, 2016, Chapter 11, pp. 11–18.